

横浜国立大学理科紀要

第一類 数学 物理学 化学

第五輯

SCIENCE REPORTS OF THE YOKOHAMA NATIONAL UNIVERSITY

SECTION I
MATHEMATICS, PHYSICS
CHEMISTRY

No. 5

FACULTY OF LIBERAL ARTS AND EDUCATION
YOKOHAMA NATIONAL UNIVERSITY
KAMAKURA, JAPAN

SEPT., 1956

The "Science Reports of the Yokohama National University" is issued in two sections:

Section I.—Mathematics, Physics, Chemistry

Section II.—Biological and Geological Sciences

Publishing Committee

Prof. Tokio Shikama, Chairman

Prof. Yosio Mutō

Prof. Keiichi Shibata

Prof. Takao Matsudaira

All communications relating to these reports should be addressed to the Chairman of the Committee.

On n -dimensional projectively flat spaces admitting a group of affine motions of order $r = n^2 - n + 1$.

By

Yosio MUTO

Introduction

In a previous paper [4]¹⁾ the present author obtained the

THEOREM A. *A necessary and sufficient condition that a curved projectively flat n -dimensional manifold A_n with symmetric affine connection admit a complete group of affine motions G_r of order $r > n^2 - n$ is that the curvature affinor belong to one of the following three types T1, T2 and T3, where the vectors satisfy the adjunct equations. Such connections and the groups really exist.*

The curvature affinor

$$(1) \quad T1: R^\lambda_{\mu\nu\omega} = aA_\mu(\delta^\lambda_\nu A_\omega - \delta^\lambda_\omega A_\nu),$$

$$a = \pm 1, A_\mu \neq 0,$$

$$(2) \quad T2: R^\lambda_{\mu\nu\omega} = aA_\mu(\delta^\lambda_\nu A_\omega - \delta^\lambda_\omega A_\nu)$$

$$+ 2\delta^\lambda_\mu(A_\nu B_\omega - A_\omega B_\nu) + \delta^\lambda_\nu(A_\mu B_\omega - A_\omega B_\mu)$$

$$- \delta^\lambda_\omega(A_\mu B_\nu - A_\nu B_\mu),$$

$$a = \pm 1, A_\mu \text{ and } B_\mu \text{ are linearly independent,}$$

$$(3) \quad T3: R^\lambda_{\mu\nu\omega} = aA_\mu(\delta^\lambda_\nu A_\omega - \delta^\lambda_\omega A_\nu) + bB_\mu(\delta^\lambda_\nu B_\omega - \delta^\lambda_\omega B_\nu),$$

$$a, b = \pm 1, A_\mu \text{ and } B_\mu \text{ are linearly independent.}$$

The adjunct equations

for T1

$$(4) \quad A_{\mu;\nu} = \alpha A_\mu A_\nu,$$

$$(5) \quad \alpha_{,\nu} = f(\alpha) A_\nu,$$

for T2

$$(6) \quad \begin{cases} A_{\mu;\nu} = (2a A_\mu A_\nu + A_\mu B_\nu - A_\nu B_\mu) \gamma \\ B_{\mu;\nu} = A_\mu C_\nu + a \gamma A_\nu B_\mu - \gamma B_\mu B_\nu, \end{cases}$$

1) Numbers in brackets refer to the references at the end of the paper.

$$(7) \quad C_{\mu;\nu} - C_{\nu;\mu} = a\gamma (A_{\mu} C_{\nu} - A_{\nu} C_{\mu}) + 2\gamma (B_{\mu} C_{\nu} - B_{\nu} C_{\mu}) + a (A_{\mu} B_{\nu} - A_{\nu} B_{\mu}),$$

$$(8) \quad a\gamma^2 = -1,$$

for T3

$$(9) \quad \begin{cases} A_{\mu;\nu} = -ab B_{\mu} C_{\nu}, \\ B_{\mu;\nu} = A_{\mu} C_{\nu}, \end{cases}$$

$$(10) \quad C_{\mu;\nu} - C_{\nu;\mu} = a (A_{\mu} B_{\nu} - A_{\nu} B_{\mu}).$$

The groups
for T1

$$(11) \quad \begin{aligned} X A_{\mu} &= 0, \quad X \alpha = 0, \\ r &= n^2, \quad \text{transitive, if } \alpha \text{ is constant,} \\ r &= n^2 - 1, \quad \text{intransitive, if } \alpha \text{ is not constant,} \end{aligned}$$

for T2

$$(12) \quad \begin{aligned} X A_{\mu} &= 0, \quad X B_{\mu} = \beta A_{\mu}, \\ r &= n^2 - n + 1, \quad \text{transitive,} \end{aligned}$$

for T3

$$(13) \quad \begin{aligned} X A_{\mu} &= -ab \beta B_{\mu}, \quad X B_{\mu} = \beta A_{\mu}, \\ r &= n^2 - n + 1, \quad \text{transitive.} \end{aligned}$$

In these equations the curvature affnor $R^{\lambda}_{\mu\nu\omega}$ is given by

$$(14) \quad R^{\lambda}_{\mu\nu\omega} = \Gamma^{\lambda}_{\mu\nu;\omega} - \Gamma^{\lambda}_{\mu\omega;\nu} + \Gamma^{\sigma}_{\mu\nu} \Gamma^{\lambda}_{\sigma\omega} - \Gamma^{\sigma}_{\mu\omega} \Gamma^{\lambda}_{\sigma\nu}$$

and X is the symbol of the Lie derivative, hence

$$(15) \quad X \Gamma^{\lambda}_{\mu\nu} = \xi^{\lambda}_{;\mu;\nu} + \xi^{\sigma}_{\mu\nu} \Gamma^{\lambda}_{\sigma\omega} - \Gamma^{\sigma}_{\mu\nu} \xi^{\lambda}_{;\sigma;\omega} + \Gamma^{\lambda}_{\sigma\nu} \xi^{\sigma}_{;\mu;\omega} + \Gamma^{\lambda}_{\mu\sigma} \xi^{\sigma}_{;\nu;\omega}$$

for the connection parameters $\Gamma^{\lambda}_{\mu\nu}$ and

$$(16) \quad X T^{\lambda\cdots}_{\mu\cdots} = \xi^{\sigma}_{\mu\cdots} T^{\lambda\cdots}_{\sigma\cdots;\omega} - T^{\sigma\cdots}_{\mu\cdots} \xi^{\lambda}_{;\sigma;\omega} - \cdots + T^{\lambda\cdots}_{\sigma\cdots} \xi^{\sigma}_{\mu;\omega} + \cdots$$

for an affnor $T^{\lambda\cdots}_{\mu\cdots}$, the semicolon denoting the covariant derivative. As we consider that the connection is without torsion, we have

$$(17) \quad \xi^{\lambda}_{\mu} = \xi^{\lambda}_{;\mu},$$

and, a group of affine motions being a group generated by infinitesimal transformations with the vectors ξ^λ satisfying

$$(18) \quad XI_{\mu\nu}^\lambda = 0,$$

we have [5]

$$(19) \quad \xi_{\mu;\nu}^\lambda = -R_{\mu\nu\alpha}^\lambda \xi^\alpha.$$

The spaces of type T1 stated in this theorem were studied by I.P. Egorov and also by the present author [2, 3, 4]. Hence we study the spaces of type T2 and type T3 in the present paper.

§ 1. The spaces of type T2.

For the spaces of type T2 we have (6), (7) and (8). But we find from (2) that the vector B_μ is not uniquely determined, a transformation of the form

$$(20) \quad \begin{cases} \tilde{A}_\mu = A_\mu, \\ \tilde{B}_\mu = B_\mu + \lambda A_\mu \end{cases}$$

being admitted without changing the second member of (2). Then, as we get

$$\begin{aligned} \tilde{B}_{\mu;\nu} &= B_{\mu;\nu} + \lambda A_{\mu;\nu} + \lambda_{,\nu} A_\mu \\ &= A_\mu (C_\nu + a\gamma\lambda A_\nu - \gamma\lambda^2 A_\nu + 2\gamma\lambda \tilde{B}_\nu + \lambda_{,\nu}) + a\gamma A_\nu \tilde{B}_\mu - \gamma \tilde{B}_\mu \tilde{B}_\nu, \end{aligned}$$

we see that we must put

$$(21) \quad \tilde{C}_\mu = C_\mu + \lambda_{,\mu} + (a\gamma\lambda + \gamma\lambda^2) A_\mu + 2\gamma\lambda B_\mu$$

in order to have (6) for the new vectors \tilde{A}_μ , \tilde{B}_μ , \tilde{C}_μ .

Then we get

$$(22) \quad \tilde{C}_\mu = a\gamma \tilde{B}_\mu$$

if we take a solution λ of a system of partial differential equations

$$(23) \quad \lambda_{,\mu} = -C_\mu - \gamma\lambda^2 A_\mu + (a\gamma - 2\gamma\lambda) B_\mu,$$

which is integrable.

Hereafter the vectors \tilde{A}_μ , \tilde{B}_μ thus obtained will be simply denoted by A_μ , B_μ . Then we get

$$(24) \quad \begin{cases} A_{\mu;\nu} = 2a\gamma A_{\mu} A_{\nu} + \gamma (A_{\mu} B_{\nu} - A_{\nu} B_{\mu}), \\ B_{\mu;\nu} = a\gamma (A_{\mu} B_{\nu} + A_{\nu} B_{\mu}) - \gamma B_{\mu} B_{\nu}. \end{cases}$$

We find that these equations are valid when A_{μ}, B_{μ}, γ are replaced with $-A_{\mu}, -B_{\mu}, -\gamma$. As the second member of (2) is not changed then, we find that the same connection is admitted for the two roots of γ in (8). The connection satisfying (2) and (24) being uniquely determined by giving a and γ , a real space of type T2 admitting a group of affine motions of order $r = n^2 - n + 1$ is nothing but the space found by Egorov [1]

$$(25) \quad \begin{cases} \Gamma_{\mu\nu}^{\lambda} = -\delta_{\mu}^{\lambda} \psi_{\nu} - \delta_{\nu}^{\lambda} \psi_{\mu}, \\ \psi_1 = x^2, \quad \psi_2 = -x^1, \quad \psi_3 = \dots = \psi_n = 0. \end{cases}$$

It seems then that there is nothing to do with this space. But we shall derive the connection (25) by treating (24).

At first we find that B_{μ} is a gradient and put

$$(26) \quad B_{\mu} = g_{,\mu}.$$

Then $e^{-2\gamma g} A_{\mu}$ is also a gradient, and we can put

$$(27) \quad A_{\mu} = e^{2\gamma g} f_{,\mu}.$$

Now, the space being projectively flat, we can take a coordinate system such that

$$(28) \quad \Gamma_{\mu\nu}^{\lambda} = -\delta_{\mu}^{\lambda} \psi_{\nu} - \delta_{\nu}^{\lambda} \psi_{\mu}.$$

Then we get from (24)

$$(29) \quad f_{,\mu;\nu} = \rho_{\mu} f_{,\nu} + \rho_{\nu} f_{,\mu}$$

where

$$(30) \quad \rho_{\mu} = -\psi_{\mu} - \gamma g_{,\mu} + a\gamma e^{2\gamma g} f_{,\mu}.$$

Again, if we put

$$(31) \quad h = e^{-\gamma g},$$

we get

$$(32) \quad h_{,\mu;\nu} = \rho_{\mu} h_{,\nu} + \rho_{\nu} h_{,\mu}.$$

The vectors A_μ, B_μ being linearly independent, f and h are independent functions. As the equations (29) and (32) show that the system of partial differential equations

$$X_{,\mu} \rho_\nu = \rho_\mu X_{,\nu} + \rho_\nu X_{,\mu}$$

admits at least two solutions $X=f$ and $X=h$, we find that we must have

$$(33) \quad \rho_{\mu,\nu} - \rho_\mu \rho_\nu = 0,$$

hence

$$(34) \quad \rho = -\log(K_\alpha^1 x^\alpha + K^1).$$

Therefore we get

$$(35) \quad \begin{cases} f = -(K_\alpha^2 x^\alpha + K^2) / (K_\alpha^1 x^\alpha + K^1), \\ h = -(K_\alpha^0 x^\alpha + K^0) / (K_\alpha^1 x^\alpha + K^1). \end{cases}$$

If we effect a coordinate transformation

$$(36) \quad x^{\lambda'} = (K_\alpha^\lambda x^\alpha + K^\lambda) / (K_\alpha^0 x^\alpha + K^0),$$

with

$$\begin{aligned} x^{1'} &= (K_\alpha^1 x^\alpha + K^1) / (K_\alpha^0 x^\alpha + K^0), \\ x^{2'} &= (K_\alpha^2 x^\alpha + K^2) / (K_\alpha^0 x^\alpha + K^0) \end{aligned}$$

naturally, we find

$$(37) \quad x^{1'} = -e^{\gamma g}, \quad x^{2'} = f e^{\gamma g},$$

hence from (26) and (27)

$$\begin{aligned} A_{1'} &= x^{2'}, \quad A_{2'} = -x^{1'}, \quad A_{3'} = \dots = A_{n'} = 0, \\ B_{1'} &= 1/\gamma x^{1'}, \quad B_{2'} = B_{3'} = \dots = B_{n'} = 0. \end{aligned}$$

ψ is changed, while the form of (28) is not changed by the transformation (36).

This shows that, if we take a suitable coordinate system, we have, besides (28),

$$(38) \quad \begin{cases} A_1 = x^2, \quad A_2 = -x^1, \quad A_3 = \dots = A_n = 0, \\ B_1 = 1/\gamma x^1, \quad B_2 = B_3 = \dots = B_n = 0, \end{cases}$$

and moreover

$$g = (1/\gamma) \log(-x^1), \quad f = -x^2/x^1,$$

by virtue of (37).

Putting $\mu = a (= 3, \dots, n)$, $\nu = 1$ in (29), we get $\rho_a = 0$, hence $\psi_a = 0$ from (30). Putting $\mu = \nu = 2$, we get $\psi_2 = -a\gamma x^1$, and, putting $\mu = 1$, $\nu = 2$, we get $\psi_1 = a\gamma x^2$. Hence we get

$$(39) \quad \psi_1 = a\gamma x^2, \quad \psi_2 = -a\gamma x^1, \quad \psi_3 = \dots = \psi_n = 0.$$

As we have $a = -1$ for the real space, we have the connection of Egorov by taking the root $\gamma = -1$. Thus we get the

THEOREM 1. *A necessary and sufficient condition that a projectively flat manifold A_n , $n \geq 3$, with symmetric affine connection and with asymmetric Ricci tensor admit a group of affine motions of order $r = n^2 - n + 1$ is that the connection parameters satisfy*

$$\begin{aligned} \Gamma_{\mu\nu}^\lambda &= -\delta_\mu^\lambda \psi_\nu - \delta_\nu^\lambda \psi_\mu, \\ \psi_1 &= a\gamma x^2, \quad \psi_2 = -a\gamma x^1, \quad \psi_3 = \dots = \psi_n = 0 \end{aligned}$$

with

$$a\gamma^2 = -1, \quad a = \pm 1$$

in some coordinate system. As regards the real space we can consider that

$$a = -1, \quad \gamma = -1.$$

In the following this space is denoted by R1.

It seems as if we can consider only the region $x^1 < 0$ because of $g = (1/\gamma) \log(-x^1)$. Besides, (38) shows that the points $x^1 = 0$ are singular points. But these are not singular points of the space and a point with $x^1 < 0$ is taken into a point with $x^1 = 0$ or $x^1 > 0$ by a transformation of the group under consideration. As we get

$$\begin{aligned} R_{11} &= (n-1)(x^2)^2, \\ R_{12} &= n+1-(n-1)x^1x^2, \\ R_{21} &= -n-1-(n-1)x^1x^2, \\ R_{22} &= (n-1)(x^1)^2 \end{aligned}$$

from (25), hence $A_\mu = 0$ for

$$(40) \quad x^1 = 0, \quad x^2 = 0,$$

the points with (40) are singular points in the sense that the formula (2)

does not hold good. We shall find in § 5 that (40) is invariant by the transformation of the group, and it is not unreasonable to remove such points from R1.

§ 2. The space of type T3 with $a = b = 1$.

For T3 we have (9) and (10). In the case of $a = b = 1$ the second member of (3) is an invariant of the transformations

$$\begin{aligned}\tilde{A}_\mu &= \cos \theta A_\mu + \sin \theta B_\mu, \\ \tilde{B}_\mu &= -\sin \theta A_\mu + \cos \theta B_\mu,\end{aligned}$$

and we get

$$\tilde{C}_\mu = C_\mu - \theta_{,\mu}$$

by replacing A_μ, B_μ, C_μ with $\tilde{A}_\mu, \tilde{B}_\mu, \tilde{C}_\mu$. If θ is a solution of

$$(41) \quad \theta_{,\mu} = C_\mu - A_\mu \cos \theta - B_\mu \sin \theta,$$

we get $\tilde{C}_\mu = \tilde{A}_\mu$. (41) is easily found to be completely integrable. Consequently we can regard A_μ, B_μ as satisfying

$$(42) \quad \begin{cases} A_{\mu;\nu} = -B_\mu A_\nu, \\ B_{\mu;\nu} = A_\mu A_\nu \end{cases}$$

instead of (9), (10).

As we find from (42) that B_μ is a gradient, we put $B_\mu = g_{,\mu}$. Then $e^{-g} A_\mu$ is also a gradient and we have

$$(43) \quad \begin{cases} A_\mu = e^g f_{,\mu}, \\ B_\mu = g_{,\mu}. \end{cases}$$

If we take a coordinate system such that

$$(44) \quad \Gamma_{\mu\nu}^\lambda = -\delta_\mu^\lambda \psi_{,\nu} - \delta_\nu^\lambda \psi_{,\mu},$$

we get from (42)

$$(45) \quad \begin{cases} f_{,\mu;\nu} = (-\psi_{,\mu} - g_{,\mu}) f_{,\nu} + (-\psi_{,\nu} - g_{,\nu}) f_{,\mu}, \\ g_{,\mu;\nu} = -\psi_{,\mu} g_{,\nu} - \psi_{,\nu} g_{,\mu} + e^{2g} f_{,\mu} f_{,\nu}. \end{cases}$$

If we put

$$\begin{aligned}\rho_\mu &= -\psi_\mu - g_{,\mu}, \\ h &= e^{-2g} + f^2,\end{aligned}$$

(45) becomes

$$\begin{aligned}f_{,\mu}, \nu &= \rho_\mu f_{,\nu} + \rho_\nu f_{,\mu}, \\ h_{,\mu}, \nu &= \rho_\mu h_{,\nu} + \rho_\nu h_{,\mu}.\end{aligned}$$

As $f_{,\mu}$ and $h_{,\mu}$ are linearly independent, we get

$$(46) \quad \rho = -\log (K_a^1 x^a + K^1),$$

$$(47) \quad \begin{cases} f = (K_a^0 x^a + K^0) / (K_a^1 x^a + K^1), \\ h = (K_a^2 x^a + K^2) / (K_a^1 x^a + K^1). \end{cases}$$

If we effect a coordinate transformation of the form

$$x^{\lambda'} = (K_a^\lambda x^a + K^\lambda) / (K_a^0 x^a + K^0),$$

we get $x^{1'} = 1/f$, $x^{2'} = h/f$. Hence, if the new coordinates thus obtained are simply denoted by x^λ , we get

$$(48) \quad x^1 = 1/f, \quad x^2 = h/f; \quad f = 1/x^1, \quad g = \log x^1 - \frac{1}{2} \log (x^1 x^2 - 1)$$

and

$$(49) \quad \begin{cases} A_1 = -\frac{1}{x^1 (x^1 x^2 - 1)^{1/2}}, \quad A_2 = \dots = A_n = 0, \\ B_1 = \frac{x^1 x^2 - 2}{2x^1 (x^1 x^2 - 1)}, \quad B_2 = -\frac{x^1}{2(x^1 x^2 - 1)}, \\ B_3 = \dots = B_n = 0. \end{cases}$$

(44) remains valid and we obtain from (45)

$$(50) \quad \begin{cases} \psi_1 = \frac{x^2}{2(x^1 x^2 - 1)}, \quad \psi_2 = \frac{x^1}{2(x^1 x^2 - 1)}, \\ \psi_3 = \dots = \psi_n = 0. \end{cases}$$

In the real space the coordinates must satisfy

$$(51) \quad x^1 x^2 - 1 > 0.$$

Thus we get the

THEOREM 2. *A necessary and sufficient condition that a projectively flat*

manifold A_n , $n \geq 3$, with symmetric affine connection and with symmetric Ricci tensor which is non-positive admit a complete group of affine motions of order $r = n^2 - n + 1$ is that the connection parameters satisfy

$$I_{\mu\nu}^{\lambda} = -\delta_{\mu}^{\lambda} \psi_{,\nu} - \delta_{\nu}^{\lambda} \psi_{,\mu},$$

$$\psi = \frac{1}{2} \log(x^1 x^2 - 1)$$

in some coordinate system. In the real space the coordinates must satisfy $x^1 x^2 - 1 > 0$.

Such space will be denoted by R2.

§ 3. The space of type T3 with $a = b = -1$.

In the case of $a = b = -1$ we find from (9), (10) that the system of partial differential equations

$$(52) \quad \begin{cases} \alpha_{,\mu} = C_{\mu} + \frac{1}{2}(e^{\beta} - e^{-\beta})(-A_{\mu} \sin \alpha + B_{\mu} \cos \alpha), \\ \beta_{,\mu} = -\frac{1}{2}(e^{\beta} + e^{-\beta})(A_{\mu} \cos \alpha + B_{\mu} \sin \alpha) \end{cases}$$

is completely integrable. Then, if we put

$$\begin{aligned} \tilde{A}_{\mu} &= -A_{\mu} \sin \alpha + B_{\mu} \cos \alpha, \\ \tilde{B}_{\mu} &= A_{\mu} \cos \alpha + B_{\mu} \sin \alpha, \\ \tilde{C}_{\mu} &= -C_{\mu} + \alpha_{,\mu}, \end{aligned}$$

we find that we can replace A_{μ} , B_{μ} , C_{μ} by \tilde{A}_{μ} , \tilde{B}_{μ} , \tilde{C}_{μ} in (3), (9), (10). As $\tilde{C}_{\mu} = (1/2)(e^{\beta} - e^{-\beta})\tilde{A}_{\mu}$, we get

$$\begin{aligned} \tilde{A}_{\mu;\nu} &= -\frac{1}{2}(e^{\beta} - e^{-\beta})\tilde{B}_{\mu}\tilde{A}_{\nu}, \\ \tilde{B}_{\mu;\nu} &= \frac{1}{2}(e^{\beta} - e^{-\beta})\tilde{A}_{\mu}\tilde{A}_{\nu}, \\ \beta_{,\nu} &= -\frac{1}{2}(e^{\beta} + e^{-\beta})\tilde{B}_{\nu}. \end{aligned}$$

We can think that we had such vectors \tilde{A}_{μ} , \tilde{B}_{μ} as the vectors A_{μ} , B_{μ} from the beginning. Then we get

$$(53) \quad \begin{cases} A_{\mu;\nu} = -\frac{1}{2}(e^{\beta} - e^{-\beta})B_{\mu}A_{\nu}, \\ B_{\mu;\nu} = \frac{1}{2}(e^{\beta} - e^{-\beta})A_{\mu}A_{\nu}, \\ \beta_{,\nu} = -\frac{1}{2}(e^{\beta} + e^{-\beta})B_{\nu}. \end{cases}$$

As B_μ is a gradient, we can put $B_\mu = g_{,\mu}$ and get

$$(54) \quad e^\beta = -\tan(g/2).$$

Then, as $A_\mu / \sin g$ becomes a gradient, we can put

$$(55) \quad \begin{cases} f_{,\mu} = \operatorname{cosec} g A_\mu, \\ g_{,\mu} = B_\mu. \end{cases}$$

Taking a coordinate system such that

$$I_{\mu\nu}^\lambda = -\delta_\mu^\lambda \psi_\nu - \delta_\nu^\lambda \psi_\mu$$

we get

$$(56) \quad \begin{cases} f_{,\mu,\nu} = (-\psi_\mu - (\cot g) g_{,\mu}) f_{,\nu} + (-\psi_\nu - (\cot g) g_{,\nu}) f_{,\mu} \\ g_{,\mu,\nu} = -\psi_\mu g_{,\nu} - \psi_\nu g_{,\mu} + \sin g \cos g f_{,\mu} f_{,\nu}. \end{cases}$$

Now, let us try to find the functions $X(f, g)$ of f, g such that

$$(57) \quad X_{,\mu,\nu} = \pi_\mu X_{,\nu} + \pi_\nu X_{,\mu},$$

where π_μ have the form

$$(58) \quad \pi_\mu = -\psi_\mu - \lambda f_{,\mu} - \mu g_{,\mu}.$$

Then we find that $X=F$ and $X=G$ where

$$F = \tan f, \quad G = \sec f \cot g$$

are two independent solutions of (57) if we put

$$\lambda = -\tan f, \quad \mu = \cot g.$$

Hence π_μ must satisfy

$$\pi_\mu = \pi_{,\mu}, \quad \pi = -\log(K_\alpha^0 x^\alpha + K^0),$$

and we get

$$\begin{aligned} F &= (K_\alpha^1 x^\alpha + K^1) / (K_\alpha^0 x^\alpha + K^0), \\ G &= (K_\alpha^2 x^\alpha + K^2) / (K_\alpha^0 x^\alpha + K^0). \end{aligned}$$

Effecting a coordinate transformation

$$x^{\lambda'} = (K_a^\lambda x^a + K^\lambda) / (K_a^0 x^a + K^0),$$

we get

$$x^{1'} = \tan f, \quad x^{2'} = \sec f \cot g.$$

Hence we can think that we have

$$(59) \quad x^1 = \tan f, \quad x^2 = \sec f \cot g$$

and consequently

$$(60) \quad \begin{cases} f_{,1} = \frac{1}{1+(x^1)^2}, f_{,2} = \dots = f_{,n} = 0, \\ g_{,1} = \pm \frac{x^1 x^2}{(1+(x^1)^2)^{1/2} (1+(x^1)^2 + (x^2)^2)}, \\ g_{,2} = \mp \frac{(1+(x^1)^2)^{1/2}}{1+(x^1)^2 + (x^2)^2}, g_{,3} = \dots = g_{,n} = 0. \end{cases}$$

We get also

$$\lambda = -x^1, \quad \mu = \pm \frac{x^2}{(1+(x^1)^2)^{1/2}},$$

hence

$$(61) \quad \begin{cases} \psi_1 = \frac{x^1}{1+(x^1)^2 + (x^2)^2}, \quad \psi_2 = \frac{x^2}{1+(x^1)^2 + (x^2)^2} \\ \psi_3 = \dots = \psi_n = 0. \end{cases}$$

from (58) or (56). As for the vectors A_μ, B_μ , we find

$$(62) \quad \begin{cases} A_1 = \frac{1}{(1+(x^1)^2)^{1/2} (1+(x^1)^2 + (x^2)^2)^{1/2}}, \\ A_2 = \dots = A_n = 0, \\ B_1 = \frac{x^1 x^2}{(1+(x^1)^2)^{1/2} (1+(x^1)^2 + (x^2)^2)}, \\ B_2 = -\frac{(1+(x^1)^2)^{1/2}}{1+(x^1)^2 + (x^2)^2}, \\ B_3 = \dots = B_n = 0. \end{cases}$$

Thus we get the

THEOREM 3. *A necessary and sufficient condition that a projectively flat manifold A_n , $n \geq 3$, with symmetric affine connection and with symmetric Ricci tensor which is non-negative admit a complete group of affine motions of order $r = n^2 - n + 1$ is that the connection parameters satisfy*

$$(63) \quad \begin{cases} \Gamma_{\mu\nu}^{\lambda} = -\delta_{\mu}^{\lambda} \psi_{\nu} - \delta_{\nu}^{\lambda} \psi_{\mu}, & \psi_{\mu} = \psi_{,\mu}, \\ \psi = \frac{1}{2} \log (1 + (x^1)^2 + (x^2)^2) \end{cases}$$

in some coordinate system.

Such space will be denoted by R3.

If complex numbers are admitted, this theorem can easily be derived from Theorem 2 by a transformation of the form

$$u^1 = x^1 + ix^2, \quad u^2 = -x^1 + ix^2.$$

§ 4. The space of type T3 with $a=-1$, $b=1$.

This space is obtained by replacing the first equation of (49) by

$$A_1 = -\frac{1}{x^1(1-x^1x^2)^{1/2}}.$$

(50) remains unchanged, but in the real space the coordinates must satisfy

$$x^1 x^2 - 1 < 0.$$

Thus we get the

THEOREM 4. *A necessary and sufficient condition that a projectively flat manifold A_n , $n \geq 3$, with symmetric affine connection and with symmetric Ricci tensor which is indefinite admit a complete group of affine motions of order $r = n^2 - n + 1$ is that the connection parameters satisfy*

$$\begin{aligned} \Gamma_{\mu\nu}^{\lambda} &= -\delta_{\mu}^{\lambda} \psi_{\nu} - \delta_{\nu}^{\lambda} \psi_{\mu}, & \psi_{\mu} &= \psi_{,\mu}, \\ \psi &= \frac{1}{2} \log (1 - x^1 x^2) \end{aligned}$$

in some coordinate system.

Such space will be denoted by R4.

§ 5. The group of affine motions.

For the space R1 we have

$$\begin{aligned} \Gamma_{\mu\nu}^{\lambda} &= -\delta_{\mu}^{\lambda} \psi_{\nu} - \delta_{\nu}^{\lambda} \psi_{\mu}, \\ \psi_1 &= x^2, \quad \psi_2 = -x^1, \quad \psi_3 = \dots = \psi_n = 0 \end{aligned}$$

and

$$\begin{aligned}\xi^\lambda &= x^1 \delta_2^\lambda, \\ x^2 \delta_1^\lambda, \\ x^1 \delta_1^\lambda - x^2 \delta_2^\lambda, \\ \delta_i^\lambda & \quad (i = 3, \dots, n), \\ \delta_i^\lambda x^\alpha & \quad (\alpha = 1, \dots, n)\end{aligned}$$

as Egorov has shown [1]. The finite equations of the group are

$$(64) \quad \begin{cases} x'^1 = a_1^1 x^1 + a_2^1 x^2, \\ x'^2 = a_1^2 x^1 + a_2^2 x^2, \\ x'^i = K_\mu^i x^\mu + K^i \end{cases} \quad (i = 3, \dots, n),$$

where

$$\begin{vmatrix} a_1^1 & a_2^1 \\ a_1^2 & a_2^2 \end{vmatrix} = 1.$$

For the space R^2 the group of affine motions is obtained from

$$(65) \quad X A_\mu = -\beta B_\mu, \quad X B_\mu = \beta A_\mu,$$

where $\beta_{, \nu} = X C_\nu$. As we have $C_\mu = A_\mu$ in § 2, we get $\beta_{, \nu} = -\beta B_\nu$. Hence we get

$$\beta = \frac{k_2}{x^1} (x^1 x^2 - 1)^{1/2}$$

by virtue of (49).

Because of (42) (65) becomes

$$\begin{aligned}(A_\alpha \xi^\alpha)_{; \mu} - A_\alpha \xi^\alpha B_\mu + B_\alpha \xi^\alpha A_\mu + \beta B_\mu &= 0, \\ (B_\alpha \xi^\alpha)_{; \mu} - \beta A_\mu &= 0.\end{aligned}$$

If we put

$$X = A_\alpha \xi^\alpha, \quad Y = B_\alpha \xi^\alpha,$$

we get a system of equations

$$\begin{aligned}X_{, \mu} - X B_\mu + Y A_\mu + \beta B_\mu &= 0, \\ Y_{, \mu} - \beta A_\mu &= 0,\end{aligned}$$

which admits the solution

$$X = (x^1 x^2 - 1)^{-1/2} \left(-\frac{k_2}{x^1} - k' + \frac{k_1}{2} x^1 + \frac{k_2}{2} x^2 \right),$$

$$Y = \frac{k_2}{x^1} + k',$$

for we have (49).

Then ξ^1, ξ^2 are obtained at once as

$$(66) \quad \begin{cases} \xi^1 = -\frac{k_1}{2} (x^1)^2 + k_2 \left(1 - \frac{x^1 x^2}{2} \right) + k' x^1, \\ \xi^2 = k_1 \left(1 - \frac{x^1 x^2}{2} \right) - \frac{k_2}{2} (x^2)^2 - k' x^2, \end{cases}$$

and we get

$$(67) \quad \psi_a \xi^a = \psi_1 \xi^1 + \psi_2 \xi^2 = -\frac{1}{2} (k_1 x^1 + k_2 x^2).$$

Now let us consider the equations (18). We get

$$\xi^{\lambda, \mu, \nu} = \delta_{\mu}^{\lambda} (\psi_a \xi^a)_{, \nu} + \delta_{\nu}^{\lambda} (\psi_a \xi^a)_{, \mu}$$

because of $\Gamma_{\mu\nu}^{\lambda} = -\delta_{\mu}^{\lambda} \psi_{, \nu} - \delta_{\nu}^{\lambda} \psi_{, \mu}$. Then, substituting (67) into these equations, we get

$$(68) \quad \xi^a = -\frac{1}{2} (k_1 x^1 + k_2 x^2) x^a + K_{\mu}^a x^{\mu} + K^a \quad (a = 3, \dots, n).$$

(66) and (68) give the vectors of infinitesimal transformation.

(66) generates a group of transformations in a two dimensional space. The finite equations of a subgroup generated by

$$\xi^1 = 2 - x^1 x^2, \quad \xi^2 = -(x^2)^2$$

is

$$x'^1 = \frac{x^1 + t^2 x^2 + 2t}{tx^2 + 1},$$

$$x'^2 = \frac{x^2}{tx^2 + 1}.$$

Hence the group generated by (66) contains a subgroup of projective transformations.

We can easily show that $x^1 x^2 - 1 = 0$ is an invariant of the group.

The equations (66), (68) are valid for R4, too.

Similarly, we get for R3

$$(69) \quad \begin{cases} \xi^1 = \frac{k_1}{2} (1 + (x^1)^2) + \frac{k_2}{2} x^1 x^2 + k' x^2, \\ \xi^2 = \frac{k_1}{2} x^1 x^2 + \frac{k_2}{2} (1 + (x^2)^2) - k' x^1, \\ \xi^a = \frac{1}{2} (k_1 x^1 + k_2 x^2) x^a + K_\mu^a x^\mu + K^a. \end{cases}$$

§ 6. Conclusion.

From Theorem A and Theorems 1, 2, 3, 4 we get the

THEOREM 5. *Consider a manifold A_n , $n \geq 5$, or a projectively flat manifold A_n , $n \geq 3$, with symmetric affine connection. A necessary and sufficient condition that the manifold admit a complete group of affine motions of order $r = n^2 - n + 1$ is that it be one of the spaces R1, R2, R3, R4.*

As the purpose of the present paper is to study only local properties, the global properties of the spaces are left open. But we find that in any of them ψ_μ are zero except ψ_1, ψ_2 which depend only upon x^1, x^2 . Therefore, if a suitable structure is assumed in the large, we can construct naturally a fibre bundle with $(n-2)$ -dimensional euclidean spaces as fibres and a two dimensional manifold M_2 as the base space. A point of M_2 is denoted by (x^1, x^2) and a point in a fibre over (x^1, x^2) is denoted by $(x^1, x^2, x^3, \dots, x^n)$. As ξ^1, ξ^2 depend only upon x^1, x^2 , a transformation of the group takes a fibre over (x^1, x^2) into a fibre over (x'^1, x'^2) . Hence the group is imprimitive with a system of imprimitivity composed of the fibres. The group of the bundle is the group of affine transformations. M_2 of R1 can be regarded as a euclidean space from which a point is removed. M_2 of R3 can be regarded as a projective space P_2 . M_2 of R2 can be regarded as the inside of a conic in a P_2 , while that of R4 as the outside.

References

- [1] Egorov, I. P.: Doklady Akad. Nauk (N. S.). SSSR, **87** (1952), 693-696.
- [2] Egorov, I. P.: Ibid., **89** (1953), 781-784.
- [3] Mutō, Y.: Science Reports of the Yokohama National University, Sec. I, No. **3** (1954), 1-12.
- [4] Mutō, Y.: Ibid., No. **4** (1955), 1-18.
- [5] Yano, K.: "Groups of transformations in generalized spaces." Akademeia Press (1949).

condition of surface must be researched. Now, if the surface is an emulsion of photographic plate in the air, they are thought as follows;

- i) conditions of the emulsion itself,
 - 1) kind of the emulsion,
 - 2) water content in the emulsion,
- ii) conditions of air in contact with the emulsion,
 - 3) temperature of air and atmospheric pressure or density of air,
 - 4) absolute humidity of air or water capacity (mass in grams) contained in unit volum (1 cubic meter).

In this experiment conditions of 1) and 3) were kept constant, combination or equilibrium state of 2) and 4) was varied at one series of experimental data.

In practice, when the *klydonograph* is used at high temperature and high humidity as in summer of this country, the change of Lichtenberg figures in wet state must be compared with dry one.

The writer reported in the preliminary experiment about the above condition³⁾. In the experiment, the conditioning of humidity or preservation of definite humidity, in which various kinds of saturated salt solutions were resorted to, as described in the International Critical Tables (H. M. Spencer), Vol. I. p. 67. But, in the present experiment only sulphuric acid solutions were used, for preventing the action of effects in chemical dissolution of salts.

The object of this project was to research how the Lichtenberg figures variate in shape and size. The figures were obtained by dry plate exposed in high humidity in the air, and we wish to obtain the values of correction.

This experiment also will suggest some ideas of impulse corona discharges about the humid surface.

§ 2. Apparatus and Experimental Method

(1) High tension impulse source and circuit

The electric apparatus is the same as the impulse circuit hitherto used⁴⁾, which was supplied from the half of Gaiffe-Gallot et Pillon's D.C. high tension source. See Fig. 1. Primary voltages of kenetron (K_1 , K_2) and main transformer (T) controlled by Slidac independently. For the object of minimum fluctuations of spark discharges, sphere spark gaps (G_1 , G_2) were illuminated with the ultra violet rays from a quartz mercury vapour lamp. Through the experiments, the sphere spark-gap G_1 (2.5 cm ϕ brass ball) was kept at 0.95 cm or 0.60 cm (30.0 kV or 20.6 kV, peak value at 25°C, 760 mm Hg). The sphere spark-gap G_2 (2.0 cm ϕ brass ball) used was 0.35 cm or 0.30 cm (13.3 kV or 11.5 kV, peak value at 20°C, 760 mm Hg). And always the gap kept in state of $G_1 > G_2$, so the impulse wave supplied by G_1 was formed a chopped wave

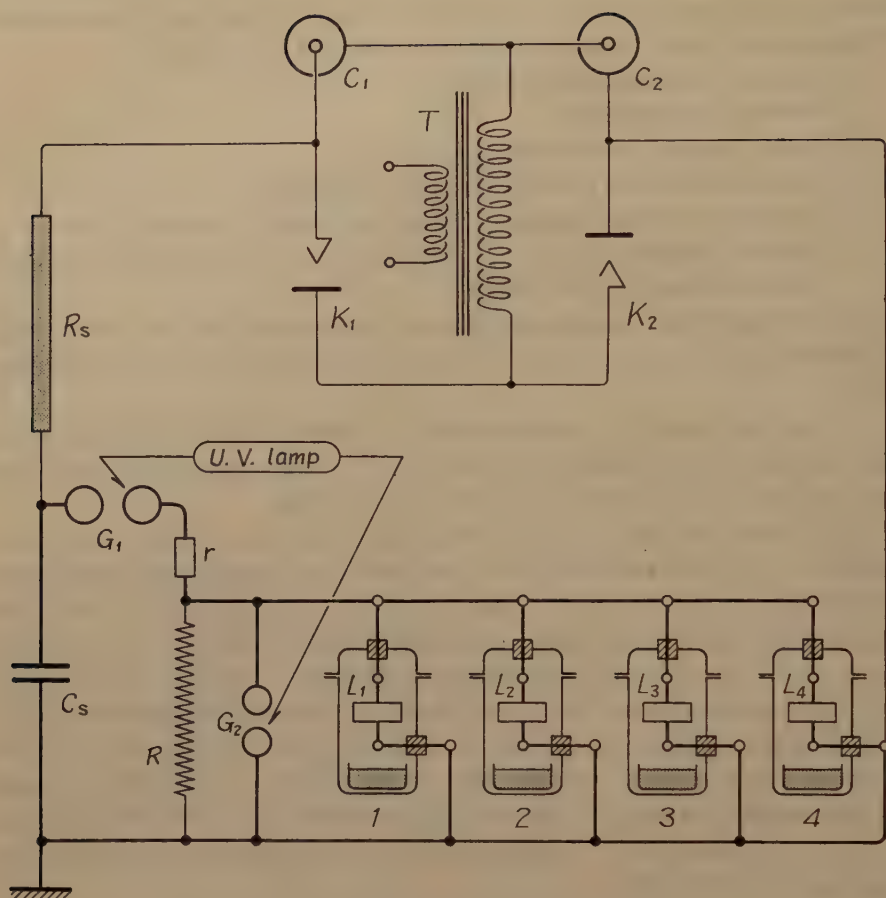


Fig. 1. Schematic diagram of the apparatus.

The circuit of Gaiffe-Gallot et Pilon's multiple rectifying high tension source, and the impulse circuit. The *klydonograph* cameras were put in the four vacuum desiccators (Nos. 1, 2, 3, 4). They were connected in parallel from sphere spark gap G_2 in the same length lead wires. Refer the former report^{3), 4)} on notations and their numerical values in this wiring diagram. L_1, L_2, L_3, L_4 : Hand made *klydonograph* cameras was put in desiccators.

Table 2.

Desiccator Nos.	1	2	3	4
Camera Nos.	1	2	3	4
% of H_2SO_4	0	30	45	50
% of R. H.	100	75	50	36

at the room temperature in 25°C.

by G_2 . The reason why the peak value about 13 kV is supplied, is that this crest voltage gives a minimum mean error in radius of positive figures ($\pm 5\%$)⁴⁾.

The terminals set up in the vacuum desiccators which contained sulphuric acid solution to maintain a definite humidity holding hand made klydonograph cameras were connected parallel so that the same shape and same crest voltage of impulse might be supplied at the same time in the positive or negative polarity. Then, the lead wires which from the terminals of G_2 to each terminal of the vacuum desiccator were used in the same length. Thus we tried to keep the other conditions than humidity as constant as possible.

(2) Humidity conditioning of photographic emulsion surface

A method of humidity conditioning was taken up as described in the Landolt-Börnstein's Tables, Vol. II, p. 1288. Refer Table 1. It shows the

Table 1. Relation between relative humidity and H_2SO_4 solutions in various temperatures.

% of H_2SO_4	temp. °C	Relative Humidity			
		0	20	25	30
0		100	100	100	100
10		96	97	96	97
20		88	87	88	88
30		74	75	75	74
40		56	55	57	58
50		33	34	36	38
60		14	16	17	18

from a part of Landolt-Börnstein's Table (Physikalisch-Chemische Tabellen Zweiter Ergänzungsband II, p. 1288).

relation between relative humidity, temperature and percentage of sulphuric acid solution. In this table, the values of relative humidity were selected as near numerical values as in the former experiment for comparison with the former one.³⁾ The selected numerical values were the ones showing the relative humidity, 100 %, 74-75 %, 50 %, 36-38 % at the room temperature in 20-30°C. The percentage of sulphuric acid solution for 50 % relative humidity would be estimated at 45 % in the room temperature of the same range.

The mixture solutions of sulphuric acid and water (0 %, 30 %, 45 %, 50 % of H_2SO_4) were put in the four vacuum desiccators (Nos. 1, 2, 3, 4) respectively. See Fig. 1, Fig. 2, and Table 2. The dry plate set up in the hand made special *klydonograph* camera, and each plate was a quarter (8.3 cm × 6.0 cm) of a cabinet size. These cameras were set up on the seven holed porcelain disk held on the shelf of the desiccators. The body of the camera was made of a pasteboard, so that the moisture of the air would reach the surface of the dry plate through it. Then, the air in contact with the emulsion surface of the dry plate would hold a definite humidity in equilibrium in 70-90 hours.

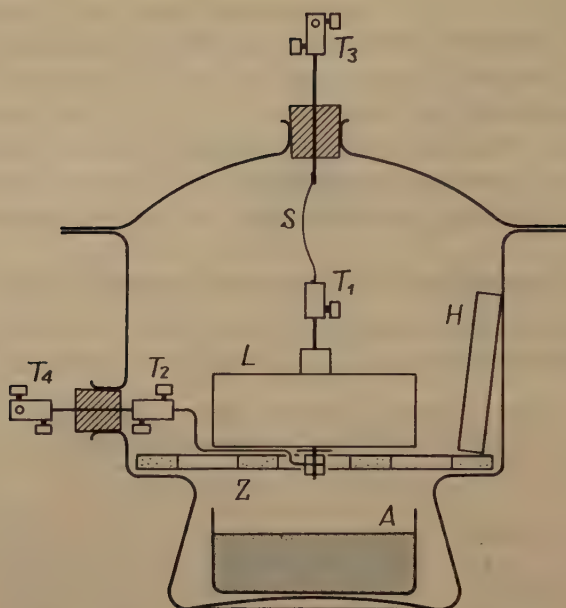


Fig. 2. *Klydonograph* camera was put in vacuum desiccator.

A: Crystalizing dish (containing the mixture of H_2SO_4 & H_2O).

L: Hand made *Klydonograph* camera.

T_1, T_2, T_3, T_4 : Terminals for camera and desiccator.

S: Brass spring wire.

H: *Ōga* hygrometer for indexing.

Z: Porcelain disk (15 cm^ϕ) with seven holes.

Through a series of the experiments, these sets were rest for so many hours. For convenience' sake, the writer treated the humidity of the moist emulsion surface with numerical value of the absolute humidity converted from the value of the relative humidity and the air temperature at that time⁵⁾.

(3) The *klydonograph* camera

The details of the camera for this experiment are shown in Fig. 3. These hand made cameras were made of a pasteboard, bakelite plate and round bar, copper plate and wire, brass vis and nuts etc.

In the first half of this experiment, a thick copper wire (0.30 cm^ϕ) was used for needle electrode, the sharp end of which was finished in the same shape. But in the second half this copper needle electrode was replaced by a special steel needle for a record of a phonograph. This object was to unify the shape of tips on the needle electrodes. So, a part of these cameras were rebuilt as shown in Fig. 4.

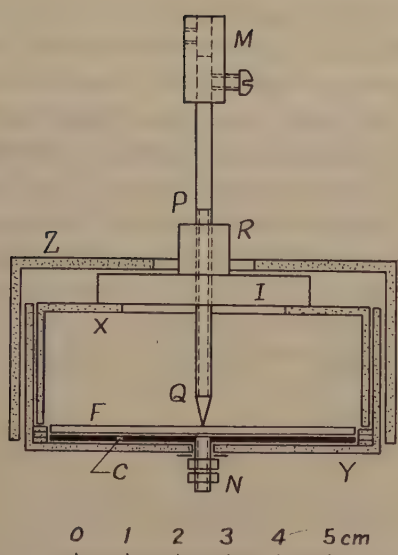


Fig. 3. Details of *Klydonograph* camera designed for this experiment.

- I: Bakelite plate (0.60 cm thick).
 R: Bakelite lock nut (1.0 cm ϕ).
 PQ: Screwed copper needle electrode (0.30 cm ϕ).
 F: Dry plate (**Fuji A1**, 1/4 cabinet size; 6.0 cm \times 8.25 cm).
 X, Y, Z: Pasteboard box, Z was double cover for mercury lamp.
 C: Copper plate electrode (6.0 cm \times 8.3 cm \times 0.10 cm).
 M, N: Brass vis and nuts (1/8" ϕ) for terminal. N was screwed and soldered in C.

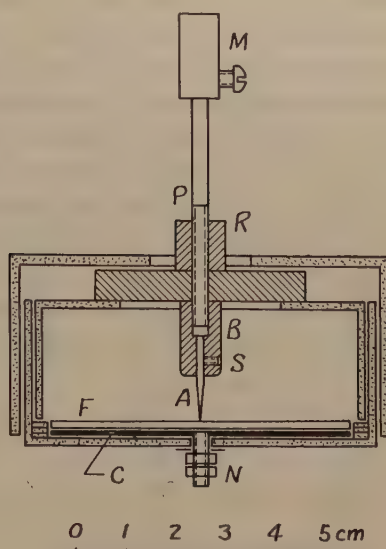


Fig. 4. Details of rebuilt camera.

- A: Special steel needle for record of phonograph (0.17 cm ϕ).
 B: Brass cap, screwed in tip of P and locked with I.
 S: Set screw for A (sunk head, 1/16" ϕ).

(4) The photographic materials and their treatment

As the photosensitive materials, **Fuji A1** (orthochromatic, high speed [daylight: ASA 20°, tungsten light: ASA 12°]) dry plates were used. As a series, these plates were a quarter of a cabinet size plate.

After an impulse supplied on these plates, the series were developed by $\text{Dk}_1^{(3)}$ at the same temperature (20°C) at the same interval (5 minutes), and fixed by FF- H_4 of the indicated fixing bath (15 minutes).

§3. Experimental Result and Measurements

Photo. 1 shows the typical examples of the positive figures (upper two rows) and negative figures (lower two rows); they were obtained by the

cameras of Fig. 3 (copper needle electrode). The crest voltage of the chopped wave of impulse at the normal state (V_n) was 13.3 kV. The first and the third rows were the series of varied humidity with positive and negative polarities, respectively. The second and the fourth rows were the series of constant humidity, and the object was to compare each figure, and to research the instrumental errors of each camera, etc. The numerical figures described under each figure were the values of given absolute humidity on each emulsion surface and surrounded air. These values converted by the calculations from

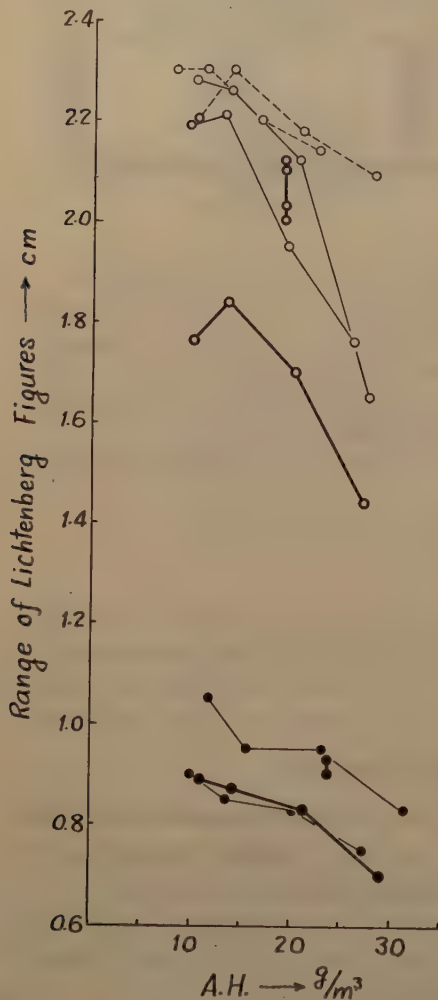


Fig. 5. Diagram of relation between range of both figures and absolute humidity. They were obtained by camera shown in Fig. 3 (copper needle electrode). $V_n=13.3$ kV.

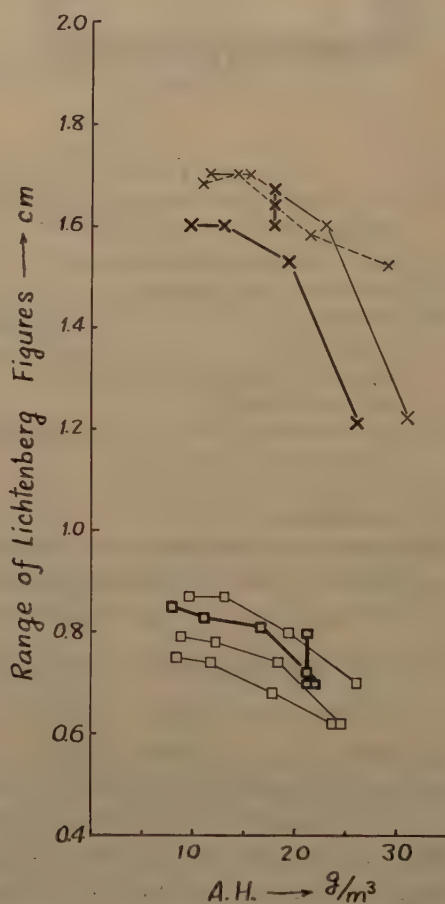


Fig. 6. Diagram of relation between range of both figures and absolute humidity. They were obtained by camera shown in Fig. 4 (special steel needle electrode). $V_n=11.5$ kV.

the room temperatures and the maintained relative humidities.

Photo. 2 shows the typical ones. They were obtained by the camera of Fig. 4 (special steel needle electrode). The arrangement and the others are the same as shown in Photo. 1. But, in these cases the flash-over on the emulsion surface often happened. So, the crest voltage of the chopped wave of the impulse at the normal state (V_n) was reduced to 11.5 kV.

The range of the positive and negative figures (the maximum length of radius from the trace touching the needle electrode) was measured on each figure respectively. The relation between the range of these figures and the absolute humidity are shown in the diagrams of Fig. 5 and Fig. 6. In these diagrams, the thick full lines are those of the examples of Photo. 1 and Photo. 2.

§ 4. Preliminary Discussion

(1) On the variation of shape and size or range of the both figures

The same tendency was recognized as that of the former report³⁾. The obtained positive figures in high humidity, in shape the dendritic streamers became wider in width, shorter in length, smaller in branches as well as in number. Also, the shape of negative figures became wider in sector width, shorter in length, smaller in the number of sectors. Refer to Photo. 1 and Photo. 2, once more.

Then, the size or range of the dendritic figures contracted as the humidity increased. The negative figures also showed the same tendency, but the effect of humidity less. This tendency became apparent beyond about 20g/m³ in absolute humidity.

The writer thought that these variations of the shape of figures were experimentally recognized as well as the figure which supplied smaller steepness in the wave front (dV/dt)⁶⁾. Also, the writer found the two following reasons in the variations of the shape and the size of the both figures. In the high humid condition, the water molecules were rich in the gelatine film of exposed emulsion surface and its surrounding air. There would be a capture of the electrons and the positive ions by rich existence of the water molecules. The capture of these charged particles by the electric impulse discharge would be a brake to stop the growth of the streamers. So the figures would be recorded smaller than the original ones.

Moreover, the dielectric constant (ϵ) of the emulsion layer would be increased by attachment of water molecules. As a result the electro-static capacity increases and the humid emulsion surface of the dry plate may be given lower voltage for an applied impulse of a constant electric charge. The size of figures depends on the function of an electric potential, or the maximum length of the streamer proportional to the applied impulse crest

voltage in some range⁶⁾. Then the size of figures contracts in the humid condition. The writer will try to confirm the above facts in experiment. In Fig. 5 and Fig. 6 positive figures may be observed to become large at about 13 g/m^3 in absolute humidity. This tendency was observed in the former experimental results. But, this enlargement may be thought the fluctuations included in these instrumental errors by the cameras and others rather than the direct effect of humidity.

(2) The rates of contraction in these figures

The rate of contraction effected by humidity in the Lichtenberg figure (II) was defined as follows by the writer:—

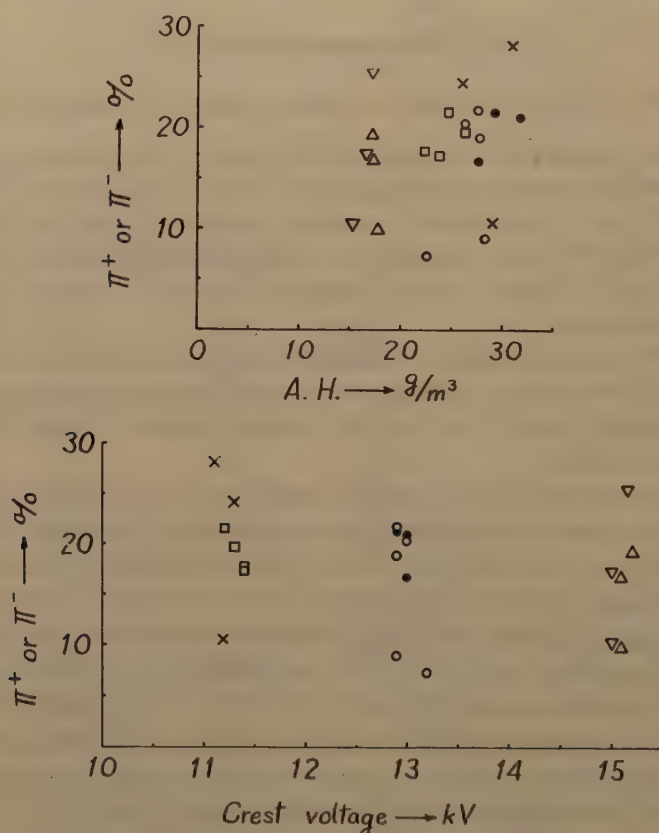


Fig. 7. Diagram of relation between given absolute humidity, applied crest voltages and rate of contractions on the both figures (π^+ , π^-).

○: ⊕ 12.9–13.2 kV } Cu ×: ⊕ 11.1–11.3 kV } S.S.
 ●: ⊖ 12.9–13.0 kV } □: ⊖ 11.2–11.4 kV }
 △: ⊕ 15.1–15.2 kV } Cu, Refer former report³⁾.
 ▽: ⊖ 15.0–15.2 kV }

$$\Pi = \frac{R_d - R_w}{R_d} \times 100 \%$$

Here, R_d was maximum radius measured in cm. at minimum humidity state. R_w was a maximum radius measured in cm. at maximum humidity.

These Π 's were calculated from the obtained data on the both figures. Fig. 7 shows a diagram relations between the given absolute humidity and the applied crest voltage and the Π^+ , Π^- . Π^+ and Π^- were the rate of contractions on the positive and negative figures respectively. The numerical values of Π^+ and Π^- were 10-30 % and 10-20 % at 25-30 g/m³ in the absolute humidity. Hence, the numerical values of correction in humid state were observed in that they were required in the above description

(3) The colored marks which appeared when special steel needle electrodes were used

When only special steel needle electrodes were used, the yellow brown colored ring marks were observed around the part of needle touching on the emulsion surface in the humid state. Photo. 3 and Photo. 4 are the typical examples of micro-photographs of the emulsion surface around the touched part of copper needle electrode in positive and negative polarity, respectively. Photo. 5 and Photo. 6 are the typical examples of micro-photographs for which the special steel needle electrode was used in both polarity. In these photos. the white part of the center in the place where the softening emulsion was shaved by the sharp end of electrode in high humidity. These micro-photographs were photographed by the posi. film and were printed. This black doughnut type ring around the white part appeared yellow brown. These rings were observed in Photo. 5 and Photo. 6, but they were not observed in Photo. 3 and Photo. 4. The outer part of these places appeared like sand a procession of the radial black spots are the groups of the developed silver particles, and they are the origin of the figures.

The writer thought that these colored marks may be a burnt place of the humid gelatine film. Because, the shape of the tip of the special steel electrode is sharper than the copper one (See Photo. 7), so the writer thought that these phenomena might depend on the difference of intensity of electric field and the different attaching state of water particles on the tip of electrode and emulsion surface (capillarity).

Also, the writer was suggested that the colored mark might be the trace of diffusion of iron ions (Fe^{++} , Fe^{+++}) from the special steel electrode⁷⁾. Clear reactions were not yet found in the results of the chemical qualitative analysis. This phenomenon may be related to the former cause.

For the next project the writer will plan to research on the effects of variated crest voltages for the highly humid plates, on the critical absolute

humidity in which either figure will change, on the applied complete impulsive wave, and effects on the materials of the electrodes at the humid emulsion layers.

This report is a part of summary of the lectures made at the Special Meeting on Discharge Physics, held by the Physical Society of Japan in Tokyo, Oct., 11, 1955.

Acknowledgements

Conclusion, the writer expresses his hearty thanks to Dr. Y. NAKAJIMA (Prof. of Y.N.U. Elect. Dept.) and Dr. T. ASAHINA (National Science Museum) who directed him throughout this work. The writer thanks also Mr. T. ONO (Tokyo Shibaura Electric Co. Ltd.) for his supply of materials etc. and Mr. T. TSUTSUMI for his cooperations in this research. April. 23. 1956.

Reference

- 1) K. Honda: Kōdenatsu Genshō (High Voltage Phenomena), Ohm-sha, p. 108-109, 1938.
- 2) Y. Toriyama: Kōatsu Denrikōgaku Genron (Fundamental Theory of High Tension Electric Engineering), Denkinotomo-sha, p. 123-131, 1938.
- 3) B. Arai: "Effect of Humidity on Lichtenberg's Figures". Natural Science and Museums, Vol. 18, No. 3, p. 57-76 (1-20), March, 1951.
- 4) B. Arai: "Study on Lichtenberg's Figures by Means of Special Dry Plates". Science Reports of the Yokohama National University, Sec. I, No. 4, p. 59-64, Oct., 1955.
- 5) Y. Kitani: Shitsudo Sokuteihō (Method of Humidity Determination), Kyōritsu-shuppan K.K., p. 1-4, 129-130, 1944.
- 6) H. Rokkaku: "Photographic Lichtenberg Figures and Their Applications". Researches of the Electrotechnical Laboratory, No. 328, p. 1-82, 1932.
J. M. Meek & J. D. Craggs: Electrical Breakdown of Gases, Oxford at the Clarendon Press, p. 215-220, 1953.
J. D. Craggs & J. M. Meek: High Voltage Laboratory Technique, Butterworths Scientific Publications, p. 289, 1954.
- 7) T. Kinbara: "Electric Figures on Photographic Plates". Ōyō Butsuri (Journal of Applied Physics, Japan). Vol. 3, No. 7, p. 245-246, 1934.

Explanations of Plate I, (1) and (2).

Date and data for Photo. 1 and 2.

Photo. No.	Row	Date	Weather	Room temp. (C°)	Atmo. press. (mm Hg)	Humidity	Polarity	V _n (kV)	V (kV)	Π ⁺ or Π ⁻
1	1	Jul. 4. 1955	Cloudy	28.2	754.4	Variated	Positive	13.3	12.9	21.7
1	2	Jun. 16. "	Rain	24.4	751.4	Constant	"	"	13.0	5.7
1	3	Jul. 25. "	Half fine	29.2	756.5	Variated	Negative	"	12.9	21.4
1	4	" 28. "	Fine	30.4	761.0	Constant	"	"	12.9	3.2
2	1	Aug. 23. "	Fine	27.2	760.6	Variated	Positive	11.5	11.3	24.4
2	2	" 15. "	"	27.8	757.0	Constant	"	"	11.2	4.2
2	3	Sep. 3. "	"	24.4	760.1	Variated	Negative	"	11.4	17.7
2	4	Aug. 14. "	Rain	27.4	756.7	Constant	"	"	11.2	12.5

V_n: Sparking peak voltage at 20°C, 760 mmHg (G₂).

V: Corrected sparking peak voltage (G₂).

The numerical figures writed under each figures were the values of given absolute humidity on each emulsion surface and surrounded air.

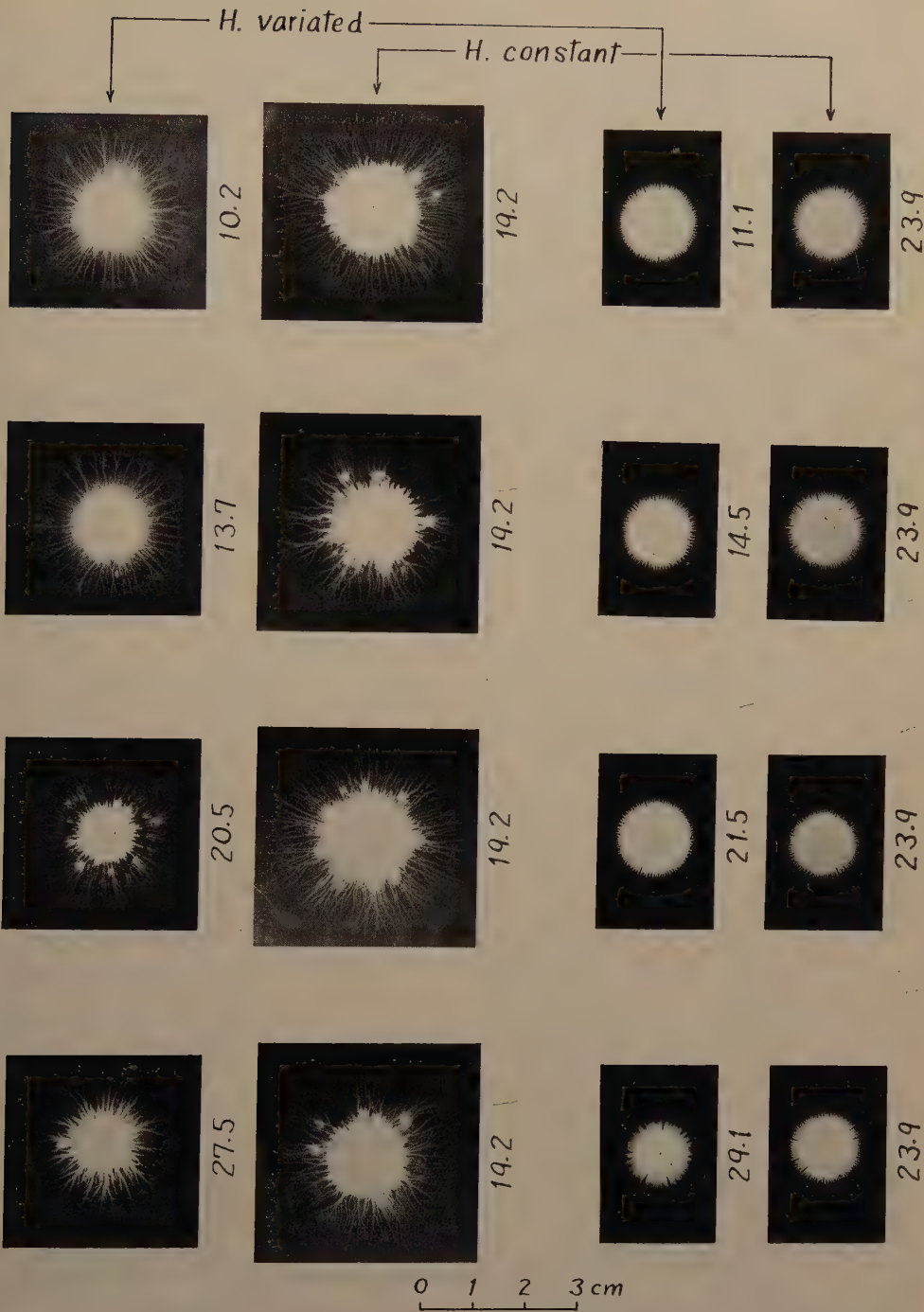


Photo. 1. Positive and negative figures obtained in various and constant humidity.
(Cu needle electrode, $V_n = 13.3$ kV).

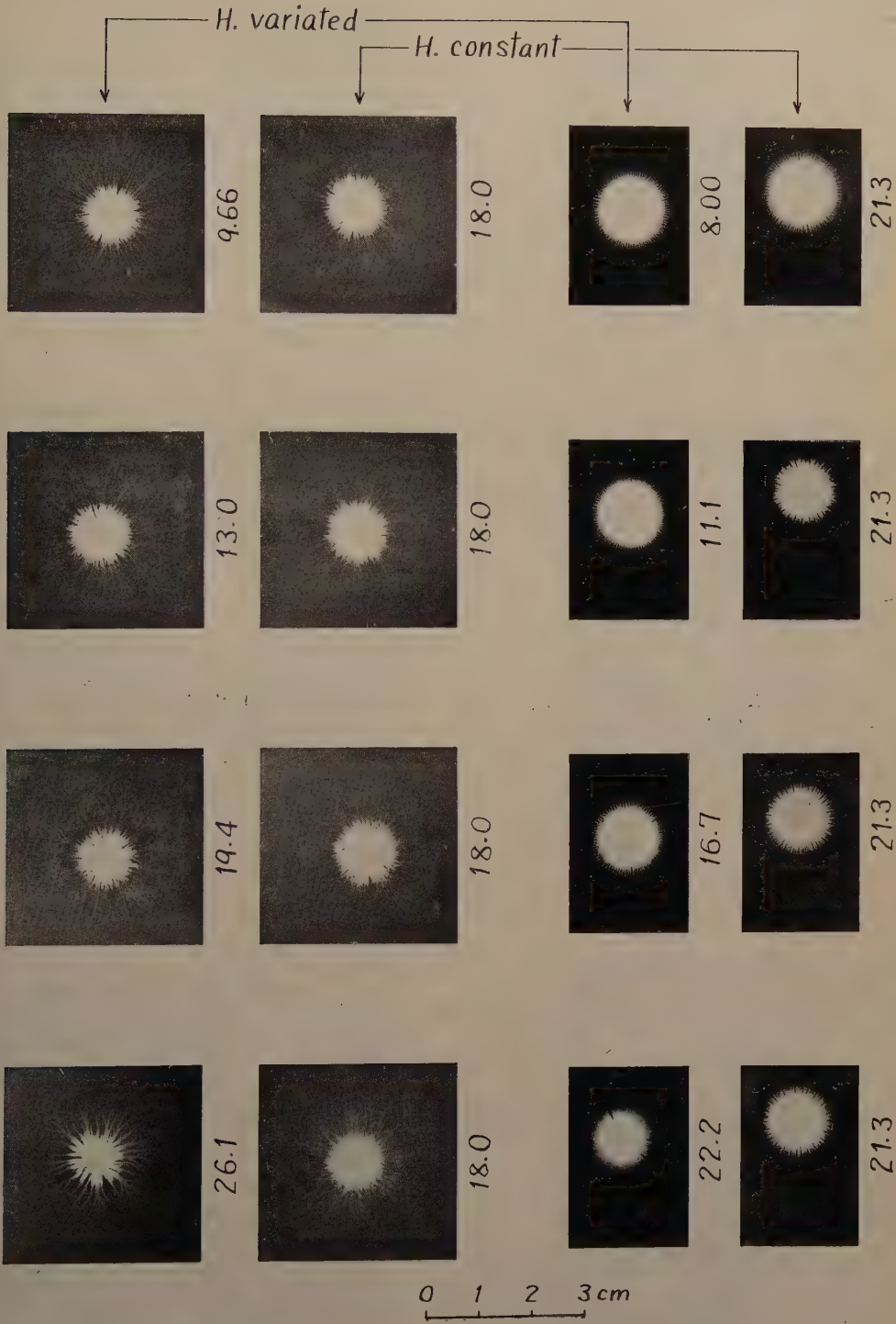


Photo. 2. Positive and negative figures obtained in various and constant humidity.
(special steel needle electrode, $V_n = 11.5$ kV).

Explanations of Plate II.

Photo. 3→6: Micro-photographs obtained around touched part of needle electrodes.
Microscope and camera: **R. WINKEL — Konica**, $\times 35$.

Photo. No.	Material of electrode	Polarity
3	Copper	+
4	"	-
5	Special steel	+
6	"	-

Photo. 7: Micro-photographs of tips of copper (1) and special steel needle electrodes (2).

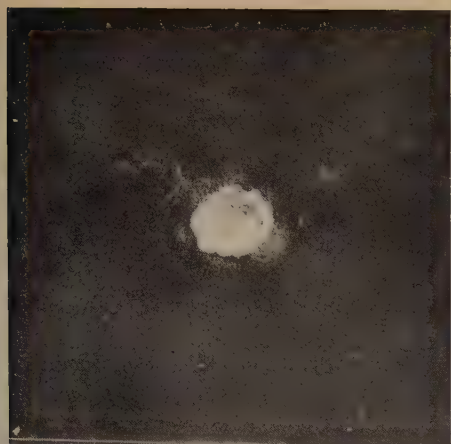


Photo. 3

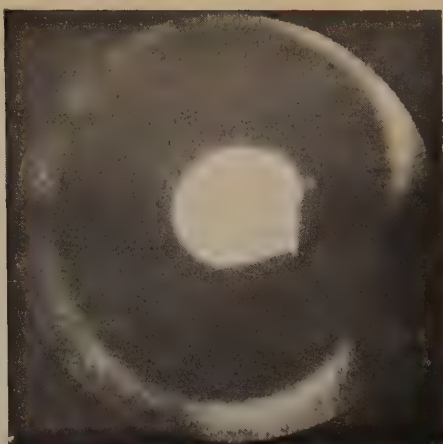


Photo. 5

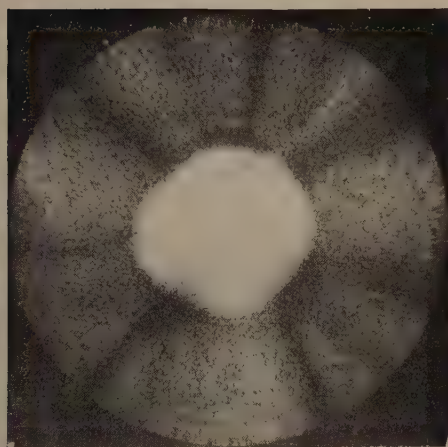


Photo. 4

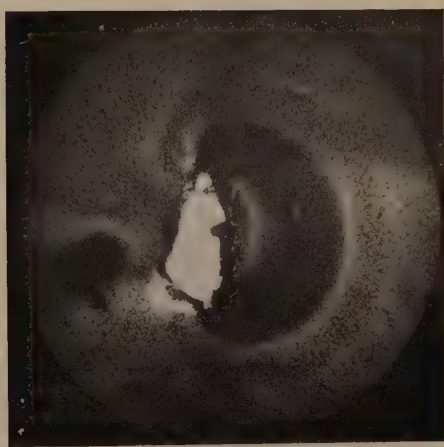


Photo. 6

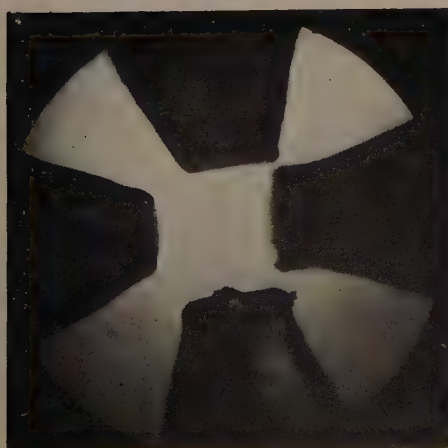


Photo. 7 (1)

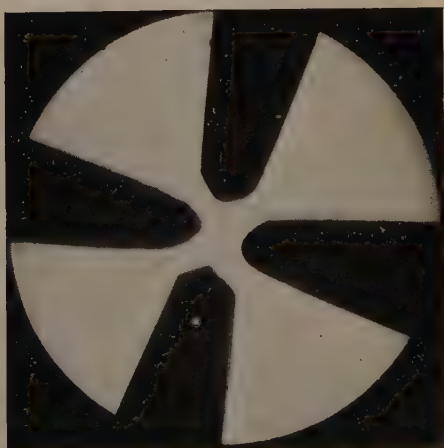
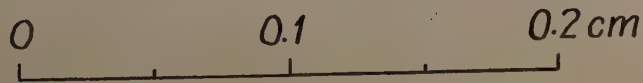


Photo. 7 (2)



Hexagonal Steps on the Surface of Fe_3O_4 solidified from the Melt

By

Nahonori MIYATA and Yasuo GONDŌ

Fe_2O_3 was melted and cooled slowly in a vacuum ($10^{-3}\sim 10^{-4}$ mm Hg) by a molybdenum-furnace. Samples changed their colour from red to black, showed strong ferromagnetic character, and had a crystal structure of spinel type. We could imagine they might be Fe_3O_4 as expected from their phase-diagram.

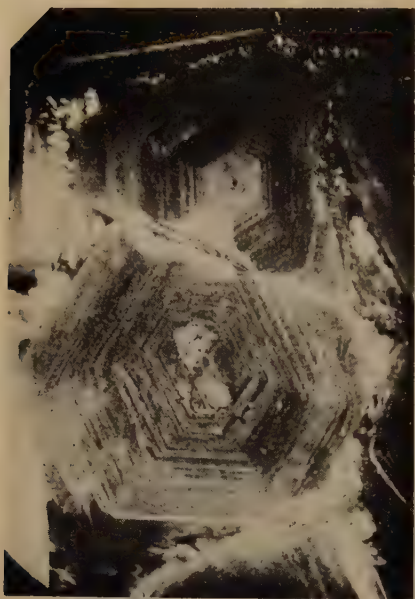
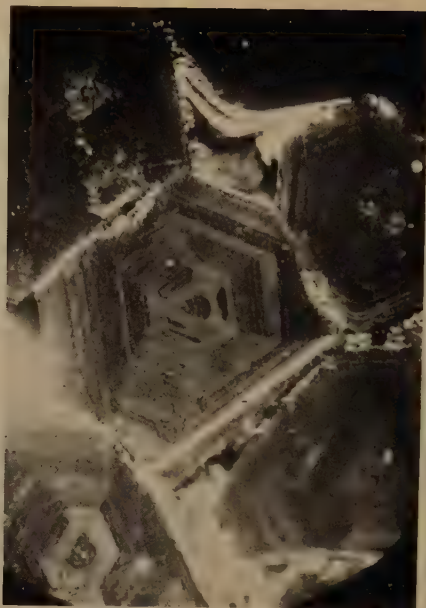
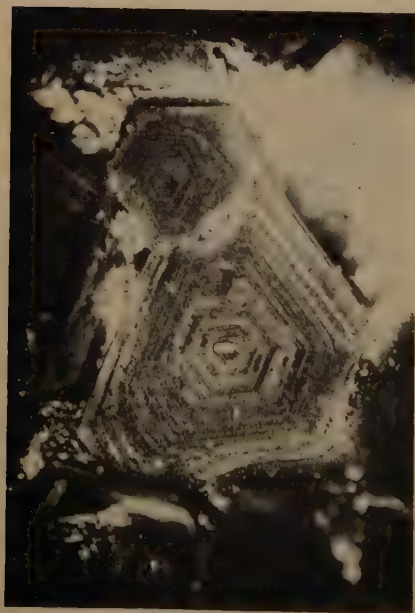
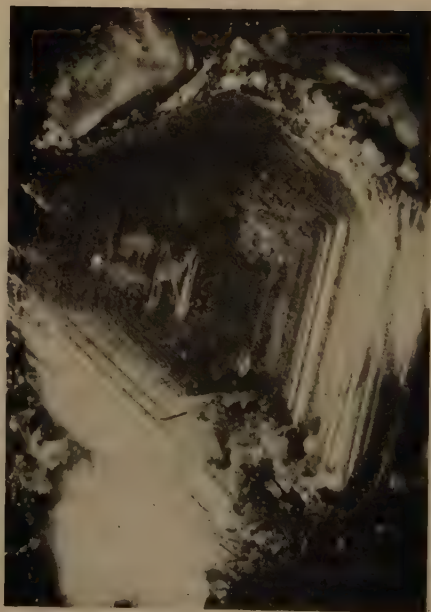
Many hexagonal plates were found on the surface. According to X-ray analysis, these plates were $\{111\}$ -planes and their hexagonal edges $\langle 110 \rangle$ -directions. They were so flat as to look very brilliant, but not exactly flat but concave, as known by the electron-microscopic shadowing method, and showed beautiful hexagonal steps under the microscopic field as seen in photographs.

From these photographs we could recognize the following results:

- 1) Two patterns, each center of which was very closely situated, grew as if they were single. (Photo. 1.)
- 2) Those, not so closely situated, were not coincident in their plane directions and seemed to disturb their growth when they met with each other. (Photo. 1, 2, 3.)
- 3) Their free edges were straight and intercrossed with an angle 120° . (Photo. 1, 2, 3, 4.)
- 4) These patterns were much larger than those found recently on some sintered materials.

The mechanism of their growth—whether they related to solidification from the melt, to condensation from the vapour, or to thermal etching, that is, evaporation from the solidified surfaces,—is not clear.

The authors wish to express their hearty thanks to Prof. Z. Funatogawa for his encouragement. This work was partly supported by the Scientific Research Expenditure from the Ministry of Education in 1955.

Photo. 1. ($\times 40$)Photo. 2. ($\times 40$)Photo 3. ($\times 40$)Photo. 4. ($\times 40$)

Precision Density Measurement of Nickel-Copper Alloys.

Part I

By

Yasuo GONDŌ, Nahonori MIYATA and Tetsuo KAMENO*

Synopsis

Densities of Ni-Cu alloys were measured by means of hydrostatic weighing method, by using the specimens which had as little macroscopic imperfections as possible. The notion to the method of the measurement is described in detail. The result shows very good agreement with that calculated from the X-ray data of the other investigator with the use of 6.023×10^{23} mole⁻¹ for Avogadro's number in chemical scale.

§ 1. Introduction

This is a preliminary report on a density measurement in several nickel-copper alloys for a hard drawn state. We have investigated a study of Young's modulus and its variation with magnetization in Ni-Cu alloys, so the density was needed for the study.

Several authors¹⁻³⁾ already reported on the density of the alloys, but their results did not agree well with each other. This is probably due to macroscopic and microscopic imperfections existing in the specimens as a result of the preparation of them, or due to the measurement with insufficient accuracy. It is well known that the density of metals decreases by cold working and the cause is supposed to be due to some microscopic imperfections—point vacancies, dislocations and grain boundaries—produced by cold working^{4, 5)}. But the decrease of density due to microscopic origin is so small, reported as the order of 10^{-4} or less, that it is not sufficient for the cause of such a remarkable variety in the observed density. Therefore, it is considered that the macroscopic imperfection—pores, voids, etc.—is one of the most important factors for the density deviation from the most closely packed state. In order to avoid the macroscopic imperfection, the preparation of the alloys from the raw materials should be carried out with great care; particularly the melting and casting of the alloys should be

* The present address: The Mutsu-ura Middle School, Mutsu-ura-machi, Kanazawa-ku, Yokohama.

carefully performed in a high vacuum.

Then the density measurement was desired to be carried on with the perfect samples as possible and with an accuracy enough to detect the microscopic imperfection.

§ 2. Specimens

Electrolytic nickel (impurities contained: Fe 0.02%, Si 0.02%, Mg 0.01%, Al 0.01%, Cu 0.01%, Mn traced) and electrolytic copper (impurities contained: Fe 0.01%, Mg 0.01%, Si 0.01%, Al 0.01%, Ca 0.01%, Ni traced) were used for the raw materials. They were melted together by means of a high frequency induction furnace in a vacuum of 10^{-3} mmHg, fully out-gased, and cast into a steel mold of 15 mm in diameter in the same vacuum, with the courtesy of Mr. T. Nagashima at the Electro-technical Laboratory⁶⁾. Then they were hot-rolled up to 8 mm square at 1000°C for a short time and cold-rolled up to 4 mm square in succession. After that they were tempered at 700°C for 3 minutes and drawn into wires of 2 mm in diameter. After all, cold working for the specimens used for the measurement was 75% reduction in area. In the alloys obtained, in spite of absolute lack of Mn, cold working up to 99% reduction was possible⁶⁾.

If the charges were out-gased enough, we could obtain perfect specimens which contained very little blowholes, that is, macroscopic imperfections. Seventeen alloys with various compositions were prepared. Grain size of the specimens was about 300/mm².

§ 3. Experimental method

We adopted the method of hydrostatic weighing; a Shimazu chemical balance, 100 g maximum load on each pan, rated sensibility 0.1 mg, was used. A calibration of the set of weights was performed by the Central Inspection Institute of Weights and Measures. For volume determination the specimens were suspended on a Nylon thread (0.04 mm in diameter) from the right pan and submerged in the water. Since the samples used were a bundle of wires, the holder of the samples took the shape of a hook with a weight (about 10 g) under it, minimizing the damping.

In order to obtain the highest precision the measurements were carried on by the next procedures.

- (1) Firstly, the weight of the sample W_{to} was measured in air, taking off the sample holder.
- (2) Secondly, the sample holder was hung in water and the weight of the sample W_l was again measured in air; in general $W_{to} \neq W_l$.
- (3) Lastly, the sample was held on the sample holder in water, and the weight of the sample W_f in water was measured.

Then, the following formula was used to calculate the density of the sample, ρ :

$$\rho = \frac{W_{lo}}{W_l - W_f} \cdot \rho_w \cdot \left(1 - \frac{W_{lo}}{W_l - W_f} \cdot \frac{\rho_a}{\rho_b} \right)$$

where ρ_w =density of water at the temperature during the measurement,
 ρ_a =density of air " " "
 ρ_b =density of the brass weight " " "

In order to determine the density within error by 10^{-4} , we must consider the next corrections for the observed values.

(1) The correction for the observed values of W_{lo} , W_l and W_f .

They should be corrected by the corrections for the weights and for the arms of the balance. Here the absolute value of the set of weights have been accurately determined to the order of 0.1 mg and the correction value of the arms is 4.3×10^{-5} .

(2) The correction for the water density ρ_w .

The standard water density is $\rho_{4^\circ\text{C}} = 1.000000 \text{ g/cm}^3$ ⁷⁾ and the temperature effect is $\Delta\rho_w = 2 \times 10^{-4}/^\circ\text{C}$.⁷⁾ Since the change of temperature is within 0.1°C during the experiment, the effect is only the order of 10^{-5} and practically may be neglected. Dissolved air effects in the 7th decimal place⁸⁾.

(3) The correction for the buoyancy of air.

This consideration is necessary, for $\frac{W_{lo}}{W_l - W_f} \cdot \frac{\rho_a}{\rho_b} \approx 1.3 \times 10^{-3}$. Then this correction value should be accurately estimated to the order of 10^{-4} . It is sufficient for the above accuracy that the adopted value of brass density is 8.4. The temperature effect of the air density is $\Delta\rho_a = 4 \times 10^{-6}/^\circ\text{C}$ ⁹⁾; for ordinary temperature fluctuation below 1°C during the experiment, it is not necessary to consider the effect. The pressure effect of the air density is $\Delta\rho_a = 1.5 \times 10^{-6}/\text{mmHg}$ ⁹⁾; for ordinary pressure fluctuation, the pressure effect is also out of question. For the humidity effect, it is sufficient that the density of water vapor, $2 \times 10^{-5} \text{ g/cm}^3$, is added to that of dry air at the temperature⁹⁾. The carbon dioxide effect⁹⁾ can be neglected.

(4) The correction for the hanging thread.

The correction for the buoyancy of water is about $1.2 \times 10^{-5} \text{ g}$, when the thread is 0.04 mm in diameter and is soaked into the water oscillatorily up and down about 1 cm. The effect of the surface tension of water against the thread is probably $1 \times 10^{-3} \text{ g}$, but in the present method, where the weight is measured three times, W_{lo} , W_l and W_f , this can be cancelled out.

(5) The correction for the sample holder.

The total volume of the sample holder is about 1.5 cm^3 , and therefore the temperature effect can not be neglected. In our method, however, it should be cancelled out and it is not necessary to consider as well as (4). Thus, it is recognized that the present method to measure W_{lo} , W_l and W_f , is

superior to the ordinary method to measure W_t and W_f only.

(6) Besides the systematic errors for the above corrections, the random errors for the observation of the resting point should be estimated. The reproducibility of our measurement is indicated by this error, which is actually about 1×10^{-4} .

After the specimens, which were a bundle of wires (4 cm in length, 2 mm in diameter and about 10 g in weight), were polished and washed with benzol, alcohol and distilled water and air bubbles over the surface of the samples were taken off carefully, then the densities were measured. A constant temperature bath was not used, but the temperature fluctuation in the water was less than 0.1°C which was small enough for our purpose, during the measurement.

§ 4. Results and Discussions

When we repeated the density measurement in the alloys, a few minute tubular voids was found in some specimens. Namely, after the first measurement, the surface of the specimens and then the voids were filed away with great care, and again the measurement was repeated. Consequently, in some cases, an increase of the density was found. After repeating this procedure several times, finally the density value was not increased any more, except pure copper, the preparation of which failed. Then this value of the density was considered as a most reliable value, and was called macroscopic density. The values reduced to those at 18°C are tabulated in Table 1.

Table 1. Densities of Ni-Cu alloys in g/cm^3 determined by hydrostatic weighing. The values $\rho_{18^\circ/4^\circ}$ are reduced to that at 18°C .

Standard: density of water at $4^\circ\text{C} = 1.0000007$.

Specimen number	Composition atom % Cu	Density $\rho_{18^\circ/4^\circ}$	Error $\Delta\rho$
NC 1	0.0	8.8972	$\pm 9 \times 10^{-4}$
2	7.1	8.9085	7
8	11.2	8.9130	14
3	14.0	8.9178	9
4	24.5	8.9274	21
5	28.4	8.9339	15
6	30.4	8.9344	14
10	33.8	8.9373	10
12	46.4	8.9493	16
13	56.8	8.9579	15
14	68.0	8.9588	16
15	76.2	8.9570	16
16	89.5	8.9477	12

As illustrated in Fig. 1, the density of Ni-Cu alloys increases like a parabola with the increase of the concentration of copper, shows a round maximum near 65 %-Cu and decreases again parabolically to that of pure copper. Near the maximum value a deviation from the quadratic curve is practically remarkable. Qualitatively this result agrees with those reported by several investigators. For the comparison with the present result, the observed values by Yamamoto¹⁾ and Nishiyama²⁾, and the calculated value obtained from the X-ray data by Owen and Pickup³⁾ are shown in Fig. 2. Here all the values are reduced to those at 18°C. The Yamamoto's result is a little lower in Ni-rich alloys and the maximum value is found near 73%-Cu alloy. So it is suggested that the specimens used there were probably less perfect macroscopically. The data reproduced exactly from Owen's report are much lower, as shown in the figure. It is necessary, we suggest, that the data should be recalculated under the consideration described below.

While an ordinary method for the precision determination of density is the hydrostatic weighing method which has been adopted by us, the second method is the X-ray method, where the density is determined by calculating the mass from the molecular weight and Avogadro's number, using the lattice constant for the volume determination. The former method gives the macro-

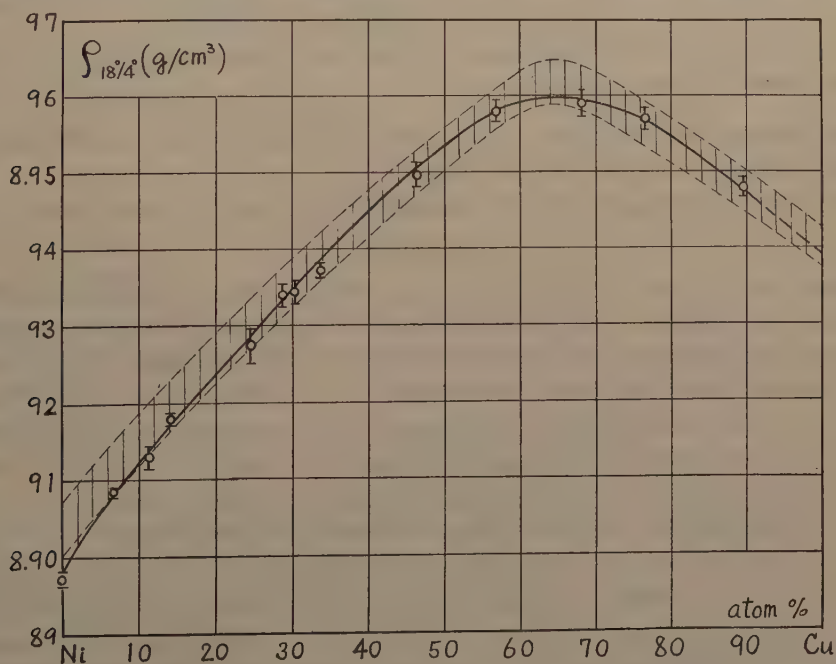


Fig. 1. Densities of Ni-Cu alloys as a function of the composition at 18°C (full line). The errors of the measurements are shown, too. The shaded band shows the densities recalculated from the Owen's X-ray data with the use of 6.023×10^{23} mole⁻¹ for Avogadro's number (chemical scale).

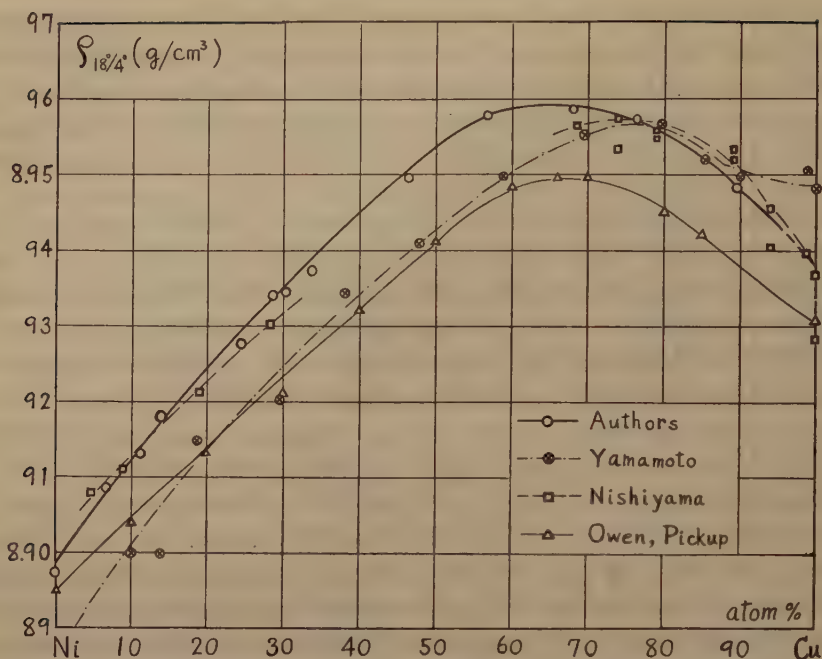


Fig. 2. Densities of Ni-Cu alloys published by several investigators. The data of Owen and Pickup are reproduced from their original report (see Fig. 1). All values are reduced to those at 18°C.

scopic density and the latter method gives the ideal density of the crystal lattice, defined as the microscopic density.

In order to determine the microscopic density, the following relation

$$\rho = 4A/Na_0^3$$

is used for the ideal crystal of the face-centered cubic structure, to which Ni-Cu alloys belong over all the compositions, where A is the molecular weight, N is Avogadro's number and a_0 is the lattice constant. While Owen and Pickup³⁾ used $1 \text{ kXU} = 1 \text{ \AA}$ for the unit of the lattice constant and $6.064 \times 10^{23} \text{ mole}^{-1}$ for Avogadro's number (Birge 1929¹⁰⁾), at present $1 \text{ \AA} = 1.00203 \text{ kXU}$ and $6.023 \times 10^{23} \text{ mole}^{-1}$ for Avogadro's number (Birge 1945¹¹⁾, DuMond and Cohen 1954¹²⁾ are recommended, respectively.

Consenuently, it is natural that the density values published by Owen and Pickup are markedly small. Now we recalculated the values using their lattice constant observed and the recommended constants and the results are shown in Fig. 1. Since the error of the lattice constant measurement is $\Delta a_0/a_0 \approx \pm 1 \times 10^{-4}$ there, so the error of the density calculated from the X-ray data is $\Delta \rho/\rho \approx \pm 3 \times 10^{-4}$ at least. This error is larger than that in our hydrostatic weighing measurement, which is shown in the figure, too, and it is shown that the recalculated curve is widely spread with the magnitude of

the error. The present result determined as the macroscopic density agrees well with the recalculated result determined as the microscopic from the X-ray data within the experimental error.

In recent years the study of the microscopic imperfection is one of the important problems of the solid-state research and such investigations have been made by various authors¹³⁾. The variation of the density due to the microscopic imperfections produced by work hardening or radiation, will not be able to be detected by the X-ray method of the above accuracy. The more accurate X-ray method is desired but the development is difficult¹⁴⁾. As the most direct method of detecting the microscopic imperfections the precision density measurement^{13, 15)} will be used better. We are now carrying on the measurement for the annealed state of the alloys, in order to study this problem, which will be published in Part II.

§ 5. Acknowledgments

We are greatly indebted to Professor Z. Funatogawa for his interest and advice in this work, to Mr. T. Nagashima and Mr. S. Hattori of the Electro-Technical Laboratory and to Mr. H. Nakae of the Tokyo Shibaura Electric Works Co. for the preparation of the alloys, and to Mr. T. Takahashi of the Central Inspection Institute of Weights and Measures for the calibration of the set of weights.

This work was partly supported by the Scientific Research Expenditure from the Ministry of Education.

References

- 1) M. Yamamoto: Nippon Kinzoku Gakkai-shi (J. Japan Inst. Metals), **5** (1941), 375 (in Japanese).
- 2) Z. Nishiyama: Sci. Rep. Tōhoku Univ., **18** (1929), 359.
- 3) E.A. Owen and L. Pickup: Z. Krist., **88** (1934), 116.
- 4) W. Boas: *Defects in Crystalline Solids* (1955), p. 212; J.F. Nicholas: Phil. Mag., **46** (1955), 87; L.M. Claerebrough, M.E. Hargreaves and G.W. West: Phil. Mag., **44** (1953), 913.
- 5) S. Issiki and H. Kimura: J. Phys. Soc. Japan, **9** (1954), 139.
- 6) T. Nagashima, T. Yamamoto and S. Hattori: Ōyō Butsuri (J. Appl. Phys. Japan), **22** (1953), 293 (in Japanese).
- 7) R.W. Tilton and J.K. Taylor: J. Res. Nat. Bur. Standards, **18** (1937), 205.
- 8) N.E. Dorsey: *Properties of Ordinary Water Substance* (Reinhold, New York, 1940).
- 9) Kishō Jyōyō-hyō (Meteorological Tables), (1927).
- 10) R.T. Birge: Phys. Rev. Suppl., **1** (1929), No. 1.
- 11) R.T. Birge: Am. J. Phys., **13** (1945), 63.
- 12) J.W.M. DuMond and E.R. Cohen: Rev. Mod. Phys., **25** (1953), 691.
- 13) See A. Smakula, J. Kalnajs and V. Sils: Phys. Rev., **99** (1955), 1747 and references 4) and 5).
- 14) A. Smakula and J. Kalnajs: Phys. Rev., **99** (1955), 1737.
- 15) A. Smakula and V. Sils: Phys. Rev., **99** (1955), 1744.

Variation of Young's Modulus with Magnetization in Single Crystals of Nickel

By

Toshirō WATANABE*, Yasuo GONDŌ and Zenya FUNATOGAWA

Synopsis

Young's modulus and its variation with magnetization (ΔE effect) of nickel crystals at room temperature were measured by a 10kc magnetostrictive vibration method. The nickel crystals were a slender cylindrical rod form. A method of growing crystals and measuring procedure with a very small driving field was described in detail. Because E_s , the value of Young's modulus at the saturated state, was the normal Young's modulus, ΔE effect should be expressed as $\Delta E/E_s$, unlike the ordinary expression. The magnetization dependence of the ΔE effect in nickel crystals was observed in a peculiar behavior (two steps, except $[111]$), similar to those of iron crystals, replacing $[100]$ in iron to $[111]$ in nickel. $(\Delta E/E_s)_r$, the value at the residual point, as a function of the orientation function was on a straight line but for $[110]$.

The elastic constants of nickel were estimated at the saturated state and well coincident with the value at 10 Mc. The values were $C_{11}=2.53$, $C_{12}=1.55$, $C_{44}=1.24$, all in units of 10^{12} dyne/cm². In the demagnetized state the elastic constants were distributed at random, as expected.

§ 1. Introduction

When tension is applied to a ferromagnetic material, the orientation of magnetic domain will be redistributed, resulting in an additional expansion besides a purely elastic one, even in an unmagnetized state. The total strain produced by the tension is the sum of the both. The magnetostrictive strain is a function of the applied stress and magnetic field. When a strong field, where the magnetization is saturated, or a strong external stress is applied, the domain magnetization vectors are completely aligned and the change in their direction cannot occur by the application of a stress and then the additional expansion disappears. This means that the measured Young's modulus, the ratio of stress to strain, of a ferromagnetic material will be a

* The present address: Department of Physics, Kōgakuin University, Shinjuku-ku, Tokyo.

function of its magnetization (and of the amplitude of stress). It is therefore expected that Young's modulus of the demagnetized state is generally smaller than that of the magnetized state. This phenomenon is usually known as the ΔE effect, first investigated experimentally by Honda¹⁾ in 1902. Since then, many reports on this phenomenon have been published. They are reviewed by Becker and Döring²⁾, and Bozorth³⁾. However, almost all the investigations have been carried on by polycrystals, so the experimental study on the ΔE effect in single crystals are very few. Only Kimura⁴⁾ measured the effect in single crystals of iron of various orientation and Yamamoto⁵⁾ also investigated on iron and nickel crystals. In nickel crystals he found peculiarities quite similar to those in the case of iron crystals. Bozorth⁶⁾ also investigated the various elastic constants of single crystals of nickel and their change with magnetization by a ultrasonic pulsing method. But further measurements in single crystals have been expected to proceed. The reason why such desired studies are few is due to the difficulty of obtaining single crystals. Now we have investigated into this problem and tried to explain the effect, based upon the conception of magnetic domains. This is the object of the present study.

As a result of the existence of the ΔE effect, a question as to what is the normal Young's modulus in ferromagnetics occurs. It should be stressed that E_s , the value at saturation, is the normal value^{6,7)}, that is, the value it could possess if the magnetostriction were zero, as Young's modulus in ferromagnetics. The value at demagnetized state, E_0 , is only for a practical use. In the demagnetized state the Hooke's law does not hold strictly and, moreover, E_0 has not always a unique value, because the distribution of the magnetic domain vectors can differ from time to time, even in the state of zero magnetization. Actually, there were remarkable fluctuations for the values of E_0 , about ± 0.6 per cent, in our measurements. On the contrary, in the saturated state the domains, accordingly E_s , are fixed; E_s is a purely elastic modulus. It should be noted that volume magnetostriction of nickel is generally so small that it can be ignored usually. Thus we take always E_s for a basic value and the customary measure of the magnitude of the ΔE effect is expressed as $\Delta E/E_s$, where $\Delta E = E - E_s$ is the difference between the values of Young's modulus at a magnetized state, E , and its value at saturated state, E_s . Of course, this expression has not an essential distinction from the ordinary expression, $\Delta'E/E_0$, with respect to the demagnetized state, where $\Delta'E = E - E_0$ and should be distinguished from ΔE . It is easily reduced to another form by the following relation, and *vice versa*,

$$\Delta'E/E_0 = [-(\Delta E/E_s) + (\Delta E/E_s)_0] \cdot [1 + (\Delta E/E_s)_0], \quad (1)$$

where $(\Delta E/E_s)_0 = (E_0 - E_s)/E_s$, the value of $\Delta E/E_s$ at the demagnetized state.

By the above reason, we should choose E_s as a starting point and measure the ΔE effect on the descending hysteresis curve. On the descending hysteresis curve, the distribution of magnetic domain at the residual point can be assumed theoretically. The following relation

$$I_r/I_s = 1/\sqrt{3} \beta_1 \quad (2)$$

is easily derived, where I_r is the magnetization at the residual point, I_s the saturation magnetization, and β_1, β_2 and β_3 are the direction cosines of the rod axis with respect to the three cubic axes, $[100]$, $[010]$ and $[001]$, respectively, in order of the magnitude. The relation (2) is held in both regions where $\beta_1 > \beta_2 + \beta_3$ and $\beta_1 < \beta_2 + \beta_3$. It should be noted that the residual is a mark point which divides the hysteresis curve into two branches—one for the higher magnetization according to “rotation” process, that is, a change in the direction of magnetization of the domains, and the other for the lower magnetization corresponding to “moving boundary” process, that is, a change in the volume of the domain. ΔE effect must be explained by these conceptions and already several theories^{2), 8-13)} have been proposed. But their experimental confirmation may not be satisfactory yet.

Measurements of Young's modulus may be performed by either a static loading or dynamical method, which gives values of the isothermal and adiabatic Young's modulus, respectively. At present rather the dynamical method has usually been adopted, because the dynamical method can give the more accurate result than the statical one and can make measurements possible by enough small stress. There are several methods of exciting longitudinal oscillations and detecting resonance, or measuring the velocity of a pulsed elastic wave. They are reviewed by Bozorth³⁾ briefly. We have adopted the method of longitudinal vibration excited magnetostrictively, as described in § 3.

§ 2. Preparation of Crystals

One way to investigate on anisotropic properties of ferromagnetic crystals is to use the single crystals, prepared for a slender cylindrical rod form with desired orientations. In another case the use of a disk form of the crystal is more desirable. For the study of ΔE effect by means of the magnetostrictive vibration, however, the former is more convenient.

As a rule, single crystals of nickel and other metals, which have no transformation in a solid phase, are usually produced from the melt by Bridgman method¹⁴⁾ (or its modified form)¹⁵⁾¹⁶⁾ and a slow cooling method¹⁷⁾¹⁸⁾. The latter one is basically simple; a suitable quantity of the material is melted in an appropriate crucible and cooled in such a way that there is a small temperature gradient along the specimen. On cooling through the melting

point the supercooled molten metal will solidify at one end and a crystal formed there will slowly grow as the rest of the material solidifies. On the other hand, the former method is founded on almost the same principle as described above, but it is an important difference between them that in the Bridgman method the lowering of solidified crystals through a freezing point from the high temperature region with a suitable speed with respect to the crystal orientation is needed. By this method, using a seed and a suitable speed for lowering crystals, it is easier to produce a crystal of the selected orientation. Furthermore, its advantage is to be able to obtain a long crystal more easily, if the so-called "zone melting" method is used together, in which only a small portion of the metal wire is melted at first and the melted region is moved gradually. Therefore we have adopted the modified method, almost the same as described by H. Takaki and others¹⁶⁾, except the construction of the furnace.

There are, however, remarkable practical difficulties in the use of this method with high melting point metals such as nickel, etc. They are those of the high temperature production and of protecting the samples and the heating element from oxidation. Those difficulties are overcome by the use of a high resistance wire-wound furnace operated in a vacuum without the use of a heavy current such as in a Tamman furnace. For the heating element a molybdenum or tungsten wire is conveniently used. A reducing atmosphere such as hydrogen is not desirable for melting nickel, because nickel absorbs hydrogen, thus producing inclusions of gas in the specimen.

(A) Furnace and method of growth.

The vertical molybdenum resistance tube furnace is shown in Fig. 1. The heater was prepared by winding a

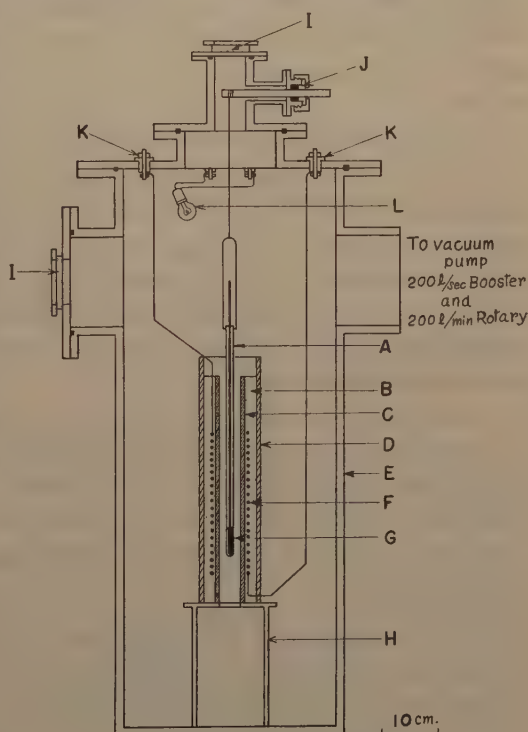


Fig. 1. Diagram of furnace

A, alumina crucible; B, pure alumina coarse powder; C, AM alumina tube; D, SM alumina tube; E, steel casing; F, molybdenum heater; G, nickel seed and wire; H, steel supporter; I, glass window; J, Wilson seal; K, heater terminal; L, lamp.

molybdenum wire (1.4 mm diameter) 50 times with 5 mm in pitch on a Tōkai Rozai AM alumina tube of 54 mm in outer diameter.

The casing, in which the furnace was mounted, was held in a vacuum, about 10^{-3} mmHg, by a OB200-booster pump during operation. The temperature was observed with an optical pyrometer through the top glass window and also was crudely estimated, using the heating element itself as a resistance thermometer. When the temperature reached 1500°C , the voltage applied to the furnace was approximately 72 V and the heating current was 22 A, then the furnace attained an equilibrium state. During the operation, the voltage had to be held constant carefully to keep the temperature constant. An alumina crucible of 3 mm in inner diameter, 7 mm in outer diameter and 40 cm in length, with a seed and a nickel wire inserted to be melted (50 cm length and 2 mm diameter), was hung at the suitable position in the furnace by a thin molybdenum wire (0.08 mm diameter), was melted at the upper part of the seed and the lower portion of the wire, and then was lowered with a suitable speed from the melting point region. The control of the lowering speed, from 4 cm/h to 20 cm/h, was attained by a synchronous motor and reduction gears. For this lowering mechanism a Wilson seal was applied.

As the seed became a nucleus for the growing of a new crystal, we could obtain the crystal with a desired orientation in most cases. Sometimes the rod produced by this procedure was divided into several crystals. Perhaps this occurred when the polycrystalline wire inserted in the crucible had not slid down smoothly. We suppose that it was due to a "thermal shock", that is, the colder polycrystalline wire dropped suddenly into the supercooled molten metal just over the growing crystal and made it to solidify with independent orientations.

After the procedure, the crucible was broken carefully by a grinder and the ingot was removed; grain boundaries between crystals in the specimen was plainly seen by etching it in a conc. HNO_3 . Its crystallographic orientation was determined by the X-ray rotation photographs. During the procedure, it was especially necessary to avoid introducing any undue strain.

(B) Specimens.

The polycrystalline nickel wire used in our study was prepared with the courtesy of Tokyo Shibaura Electric Works Co., Ltd. and impurities detected by spectroscopic analysis were Mn, Fe, Si, Mg, Al and a trace of Ca as shown in Table 1. The purity of the material was 99.6 % or more.

Table 1. Spectroscopic analysis of materials.

Si	Al	Fe	Mg	Ca	Mn
+	+	++	+	trace	++

Table 2. Dimensions, orientations and residual magnetization of the specimens. $I_{r-calc.}$ and $I_{r-obs.}$ denote the calculated and observed values of residual magnetization, respectively.

Specimen number	Length (cm)	Diameter (cm)	Direction cosines			$I_{r-calc.}$ (gauss)	$I_{r-obs.}$ (gauss)
			β_1	β_2	β_3		
No. 1	17.83	0.284	0.633	0.576	0.518	456	458
No. 2	19.72	0.289	0.795	0.602	0.073	363	375
No. 3	20.00	0.284	0.999	0.013	0.013	289	285
N 12a	18.16	0.277	0.922	0.307	0.237	313	315
N 13a	19.14	0.277	0.883	0.467	0.052	327	366
N 14a	20.90	0.278	0.958	0.223	0.178	301	294
N 15	20.04	0.279	0.996	0.091	0.000	290	285
N 17b	21.07	0.281	0.994	0.108	0.022	290	290
Polycrystal	20.20	0.197	—	—	—	—	396

All the specimens prepared were cylindrical rods and annealed at 900°C for 2 hours in a vacuum. The constants of the specimens are shown in Table 2.

I_{r-calc} and I_{r-obs} in the table are calculated values by Eq. 2 and observed values of the residual magnetization at room temperatures, respectively. Fig. 2 shows the stereographic projection of the orientations of the specimens.

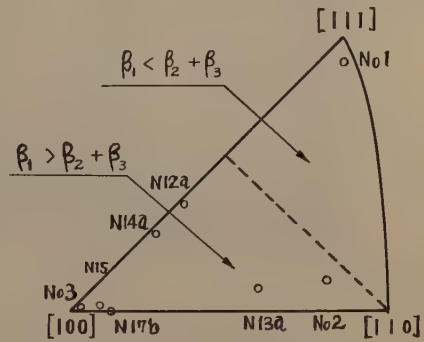


Fig. 2. Stereographic projection of the orientation of the specimens.

§ 3. Experimental Method

The Young's modulus, E , and its change ΔE due to magnetization were determined by the resonance frequency of the forced longitudinal vibration, produced magnetostrictively, and applied to the specimen¹⁹⁾²⁰⁾. The magnetic properties were measured ballistically. The magnetic field was produced by a water-jacketed solenoid, 40 cm in length, of the field constant of 59.5 Oe/A. The homogeneity of the magnetic field produced was within 2 per cent over the length of 20 cm in the central position of the solenoid.

For rods vibrating in the longitudinal mode this fundamental resonance frequency is given by the relation

$$E = 4\rho l^2 f^2 \left(1 + \frac{\pi^2 r^2 \mu^2}{2l^2} \right), \quad (3)$$

where l is the length of the rod, r the diameter of the rod, ρ its density, f

the fundamental resonance frequency and μ its Poisson ratio. Because the magnitude of the second term in the brackets of (3) is so small as the order of 10^{-5} , the relation is reduced to

$$E = 4\rho l^2 f^2 \quad (4)$$

by neglecting it. This resonance frequency f is measured as a function of the externally applied magnetic field, H_{ex} , and the value for the saturated magnetized state, f_s , is determined in high fields, where the saturation is attained. Then, the change of Young's modulus with respect to that for the saturated magnetized state can be estimated by the next formula,

$$\Delta E/E_s = 2\Delta f/f_s \quad (5)$$

Practically, this change of the resonance frequency, Δf , is measured as the change of the capacity of the variable condenser in the oscillator, illustrated below. Thus the following relation

$$\Delta E/E_s = 2\Delta C/C_s \quad (6)$$

is finally used in order to compute the change of Young's modulus, where C_s is the capacity of the variable condenser at the saturated state and ΔC is its change.

Fig. 3 shows the block diagram of the measuring system. The center of the specimen, that is, a node of the longitudinal vibration was clamped as weakly as possible on the knife edge supporter. Both ends of the specimen

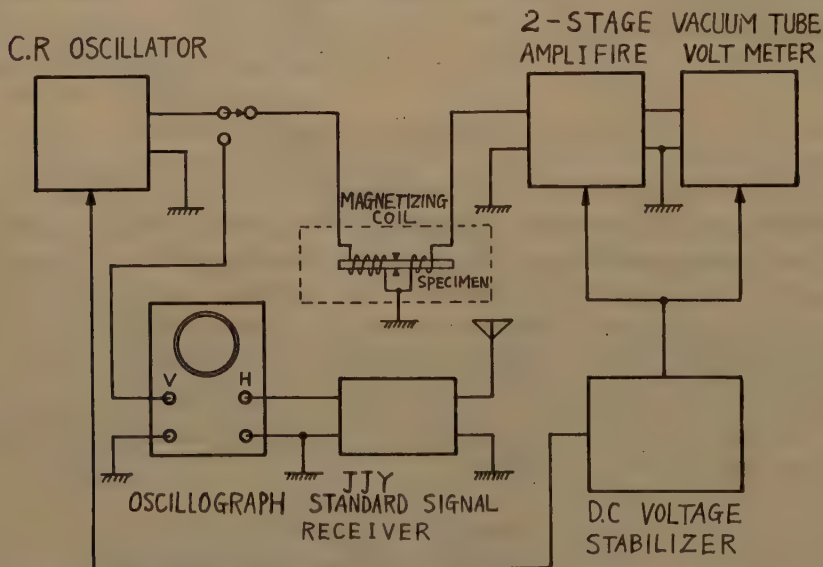


Fig. 3. Block diagram of the measuring system

were inserted into a "driving coil" and a "detecting coil", respectively, avoiding any contact with the coils, in order to prevent an obstruction against the measurement. They are illustrated by Fig. 4. The former coil was composed of a solenoid wound 500 times (B.S. #35), the length of which was 1 cm, and the latter was that wound 5000 times (B.S. #35), the length of which 2.5 cm, on each of two glass tubes of 1 cm in diameter, respectively.

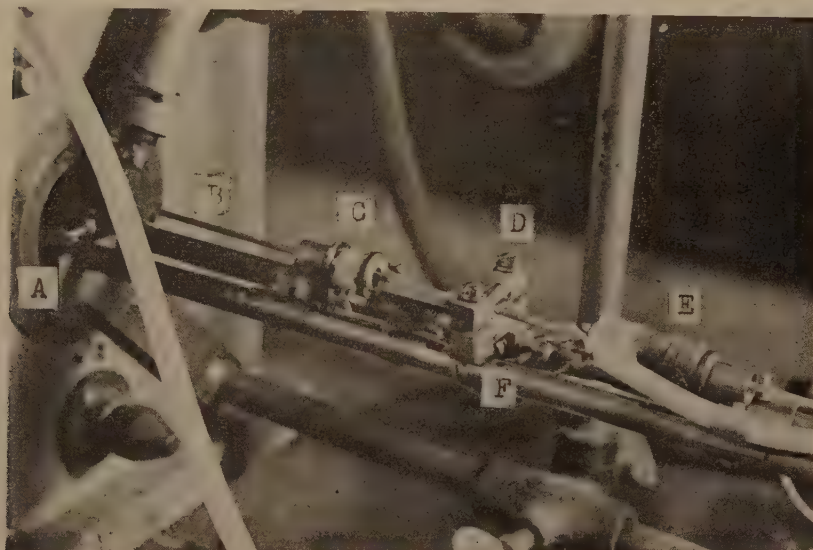


Fig. 4. Mounting of the specimen.

A, magnetizing solenoid; B, specimen (20 cm in length); C, driving coil; D, knife edge supporter; E, detecting coil; F, brass tube base.

Then they were put in the magnetizing solenoid, as shown in Figs. 3 and 4. By alternating the magnetic field of the driving coil fed by an oscillator, the longitudinal vibration was excited in the specimen.

The oscillator consisted of two parts, 6AG7—6AG7—6V6; a master oscillator, and one stage of power amplifier. The master oscillator was the modified Wien bridge type C-R circuit and was supplied by an electronically stabilized power source. A good wave form was obtained by this oscillator. The detailed circuit diagram is shown in Fig. 5. The frequency of the oscillator was calibrated by comparison with the 1000 c/sec modulated wave of the JJY Frequency Standard (4 Mc/sec).

When the specimen was vibrated magnetostrictively, the E.M.F. was induced in the detecting coil, then it was amplified and measured by a vacuum tube voltmeter. In Fig. 5 these circuits are also given in detail. The reading of a micro-ammeter (μA I in Fig. 5, the indicator of the vacuum tube voltmeter) increased steeply and showed a sharp maximum when the resonance point was reached. The capacitance of the oscillator was composed of two

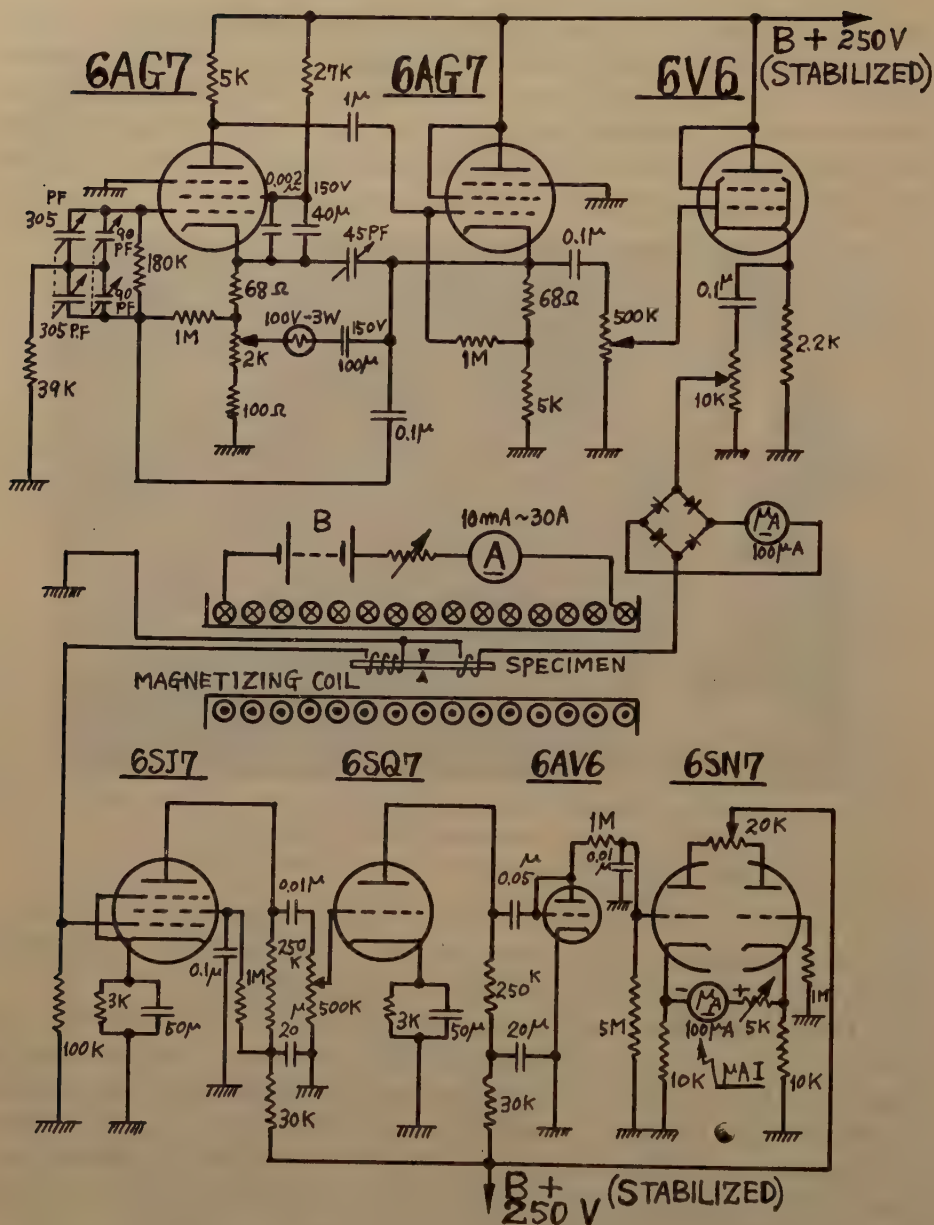


Fig. 5. Connection diagram of the apparatus.

variable condensers of different capacities connected in parallel (in order to perform fine adjustments), the total amount of the capacity being from 18 to 394 pF. The resonance point could be easily determined to one tenth of the scale division of the condenser (90 pF in full) connected in parallel, hence

to about 1/4000 of the total capacity. An example of the resonance curve is shown in Fig. 6.

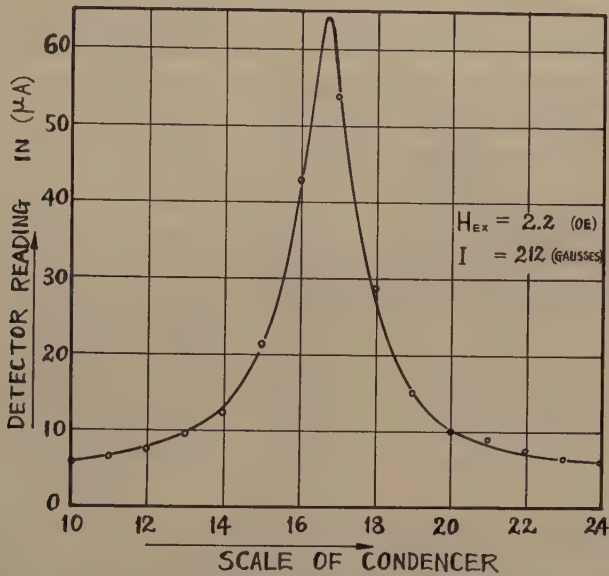


Fig. 6. An example of the resonance curve.

When such a dynamic method of magnetostrictive vibration was used, it was very necessary that the amplitude of the driving field current should be taken as small as possible. In our measurements this current was limited to $50 \mu\text{A}$, therefore, the high frequency magnetizing field produced by the current was only about 0.03 Oe in maximum. It was the most important progress on the experimental procedure that by such a small field ΔE effect could be investigated.

All the measurements were performed at the same temperature, about 18°C .

§ 4. Experimental Results

Measurements of the change of Young's modulus were carried out at several points on the descending hysteresis curve usually, at room temperature. Fig. 7 shows the change of Young's modulus relative to that for the saturated state, $\Delta E/E_s$, as a function of the magnetic field, H_{eff} . Here only those of three crystals, with principal axes, a tetragonal crystal No. 3, a diagonal crystal No. 2 and a trigonal crystal No. 1, and a polycrystal are shown. About these experimental values and those of other crystals, not shown in this figure, Tables 3 to 11 should be referred. It is noted that very remarkable anisotropy is observed. As shown there, Young's modulus of a trigonal

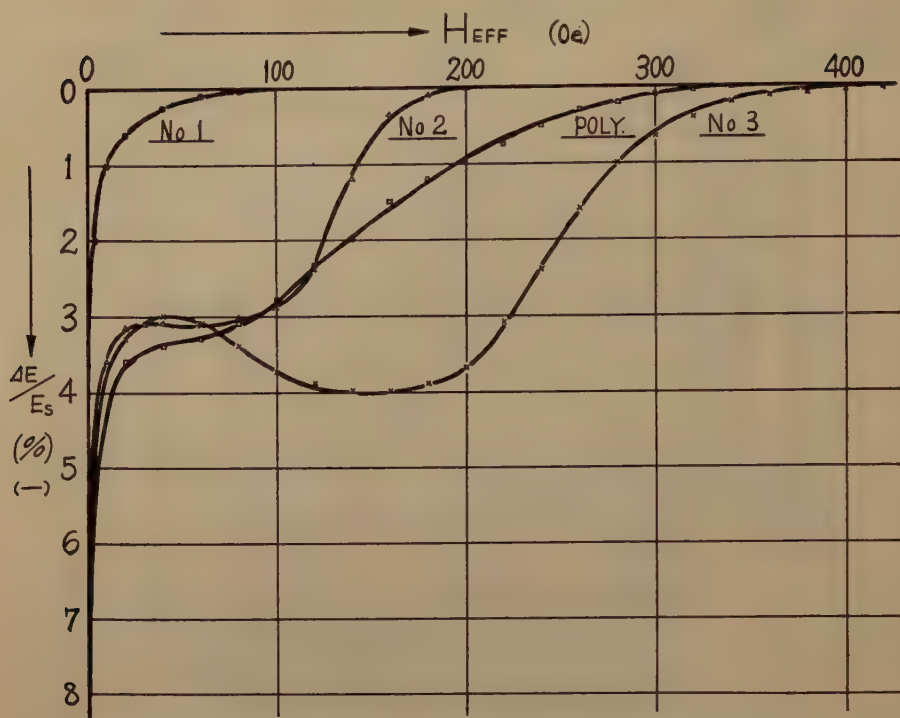


Fig. 7. Relative change of Young's modulus $\Delta E/E_s$, as a function of the magnetic field, H , in nickel crystals.

crystal, with the direction of the easiest magnetization increases quickly at low fields, but the rate of increase gradually diminishes as the field increases and finally saturates. On the other hand, in crystals with the direction of more difficult magnetization Young's modulus increases at first, has a "plateau" in the following stage, especially showing even a decrease in $[100]$, and increases again quickly just before the saturation.

In Fig. 8 and Fig. 9 the relative change of Young's modulus is shown as a function of the reduced magnetization, that is, the ratio of the intensity of magnetization, I , to the saturation magnetization, I_s , and is tabulated in Tables 3 to 11, too. Generally, Young's modulus increases gradually with the increase of magnetization, but after the magnetization exceeds the residual point, which is indicated in the figures, the rate of increase once diminishes remarkably, even showing a decrease in $[100]$, and then increases again very abruptly to the saturation. Corresponding to the field dependency, in the trigonal crystal these anomaly are not seen.

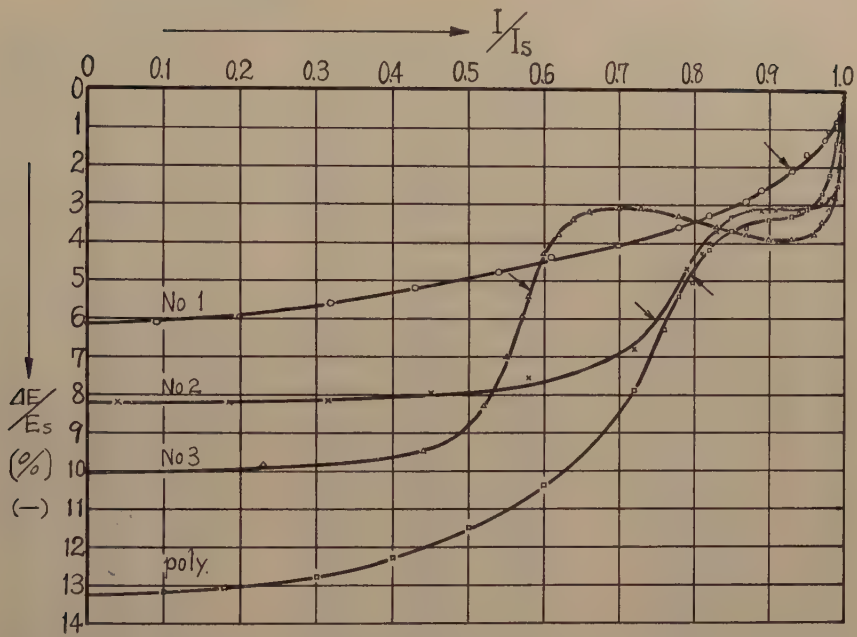


Fig. 8. Relative change of Young's modulus, $\Delta E/E_s$, as a function of the reduced magnetization, I/I_s , in nickel crystals, with the principal orientations.

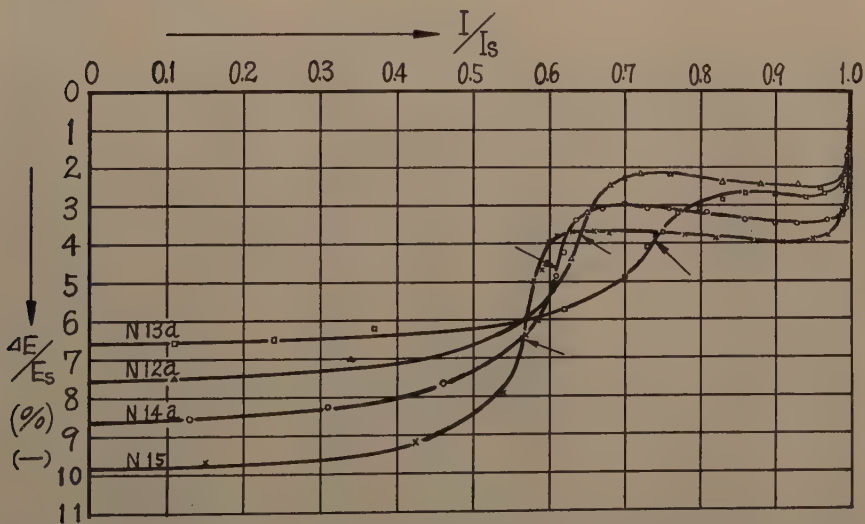


Fig. 9. Relative change of Young's modulus, $\Delta E/E_s$, as a function of the reduced magnetization, I/I_s , in nickel crystals, without the principal orientations.

Experimental values of the ΔE effect in various nickel crystals.

Table 3. No. 1

H (Oe)	I/I_s	$\Delta E/E_s$ (%)
78.5	1.000	0.00
66.5	0.999	0.02
54.6	0.998	0.14
42.7	0.997	0.24
30.8	0.996	0.43
24.8	0.995	0.53
18.9	0.993	0.65
13.0	0.987	0.84
10.0	0.983	1.06
7.12	0.975	1.25
4.36	0.952	1.66
2.60	0.926	2.05
1.57	0.894	2.65
1.11	0.865	2.94
0.72	0.824	3.26
0.36	0.775	3.64
0.13	0.702	4.05
-0.04	0.616	4.44
-0.25	0.537	4.82
-0.33	0.432	5.18
-0.37	0.319	5.60
-0.42	0.208	5.98
-0.44	0.090	6.05
-0.48	0.000	6.05

Table 4. No. 2

H (Oe)	I/I_s	$\Delta E/E_s$ (%)
191.6	1.000	0.00
174.1	0.999	0.09
162.1	0.998	0.27
150.1	0.997	0.57
138.4	0.996	1.09
126.6	0.994	2.08
114.7	0.989	2.62
102.7	0.981	2.89
90.9	0.973	2.98
67.3	0.945	3.16
43.6	0.911	3.16
31.8	0.890	3.16
20.0	0.865	3.16
14.1	0.850	3.34
8.27	0.830	3.70
5.92	0.818	4.04
4.20	0.806	4.31
2.49	0.790	4.73
1.37	0.774	6.47
0.40	0.724	6.83
-0.14	0.577	7.53
-0.19	0.453	7.95
-0.21	0.185	8.20
-0.24	0.000	8.20

Table 5. No. 3.

H (Oe)	I/I_s	$\Delta E/E_s$ (%)
411.8	1.000	0.00
387.8	0.999	0.08
364.8	0.998	0.14
340.8	0.997	0.24
316.9	0.995	0.44
293.4	0.992	0.75
269.9	0.990	1.26
245.9	0.985	2.17
233.9	0.982	2.68
221.9	0.978	3.09
209.9	0.973	3.44
197.9	0.965	3.70
186.0	0.955	3.80
162.6	0.931	3.90
139.1	0.901	3.90
115.4	0.865	3.80
91.8	0.827	3.60
68.2	0.780	3.29
44.6	0.726	3.09
32.8	0.696	3.09
21.1	0.662	3.15
15.2	0.639	3.39
9.34	0.617	3.76
6.43	0.602	4.31
3.53	0.583	5.37
2.39	0.570	5.94
1.29	0.550	6.95
0.25	0.517	8.27
-0.64	0.441	9.50
-0.84	0.227	9.90
-0.92	0.000	9.90

Table 6. N 12a

H (Oe)	I/I_s	$\Delta E/E_s$ (%)
263.1	1.000	0.00
233.6	0.999	0.16
209.6	0.998	0.65
185.6	0.997	1.79
174.1	0.995	2.12
162.1	0.993	2.39
150.1	0.986	2.45
126.6	0.962	2.53
102.9	0.925	2.45
79.4	0.877	2.45
55.8	0.826	2.39
32.3	6.760	2.21
20.6	0.723	2.21
14.7	0.702	2.29
8.89	0.678	2.55
5.98	0.664	2.61
3.09	0.646	3.11
1.94	0.637	3.59
0.80	0.625	4.41
-0.21	0.585	5.95
-0.30	0.337	6.99
-0.49	0.109	7.45
-0.52	0.000	7.45

Table 7. N 13a

H (Oe)	I/I_s	$\Delta E/E_s$ (%)
263.3	1.000	0.00
233.8	0.999	0.18
209.8	0.998	0.37
185.8	0.997	0.89
174.3	0.995	1.41
162.3	0.994	2.14
150.3	0.990	2.51
138.6	0.983	2.70
126.8	0.975	2.70
114.9	0.965	2.70
91.2	0.939	2.76
67.5	0.910	2.70
43.9	0.880	2.70
32.0	0.862	2.70
20.3	0.834	2.85
11.5	0.795	3.13
5.68	0.767	3.19
2.79	0.746	3.74
1.66	0.732	4.08
0.59	0.702	4.87
-0.23	0.616	5.73
-0.37	0.369	6.15
-0.44	0.243	6.50
-0.48	0.114	6.58
-0.58	0.000	6.58

Table 8. N 14a

H (Oe)	I/I_s	$\Delta E/E_s$ (%)
305.4	1.000	0.00
281.4	0.999	0.00
234.5	0.998	1.54
210.5	0.995	2.80
198.5	0.992	3.16
186.5	0.987	3.30
175.0	0.979	3.40
163.1	0.966	3.40
139.5	0.933	3.48
115.8	0.898	3.48
92.2	0.856	3.40
68.5	0.811	3.24
44.9	0.757	3.10
33.1	0.728	3.10
21.3	0.695	3.02
15.5	0.668	3.10
9.59	0.646	3.16
6.67	0.636	3.40
3.73	0.624	3.90
2.56	0.617	4.26
1.40	0.609	4.86
0.12	0.595	6.32
-0.43	0.462	7.66
-0.49	0.308	8.30
-0.53	0.133	8.56
-0.54	0.000	8.56

Experimental values of the ΔE effect in various nickel crystals.

Table 9. N 15

Table 10. N 17b

Table 11. Polycrystal

H (Oe)	I/I_s	$\Delta E/E_s$ (%)	H (Oe)	I/I_s	$\Delta E/E_s$ (%)	H (Oe)	I/I_s	$\Delta E/E_s$ (%)
442.3	1.000	0.00	412.3	1.000	0.00	324.9	1.000	0.00
412.3	0.998	0.10	388.3	0.999	0.11	295.4	0.999	0.16
388.3	0.996	0.24	361.3	0.998	0.19	271.9	0.998	0.31
365.3	0.935	0.34	341.3	0.997	0.43	247.9	0.997	0.47
341.3	0.992	0.54	317.3	0.996	1.03	223.9	0.996	0.72
317.4	0.990	0.94	293.8	0.995	2.07	199.4	0.994	1.00
293.9	0.988	1.54	275.3	0.994	2.77	176.4	0.992	1.28
275.4	0.985	2.34	258.3	0.993	3.35	152.4	0.988	1.72
258.4	0.977	3.24	234.4	0.987	3.63	128.9	0.978	2.12
234.4	0.970	3.84	210.4	0.977	3.74	105.0	0.967	2.68
210.5	0.955	3.94	175.0	0.945	3.74	81.3	0.950	3.12
175.1	0.920	4.04	139.5	0.895	3.63	57.6	0.926	3.25
139.6	0.875	3.94	103.9	0.840	3.56	46.7	0.910	3.37
103.9	0.822	3.84	80.3	0.795	3.35	33.8	0.892	3.46
80.4	0.782	3.84	56.7	0.748	3.14	27.9	0.877	3.56
56.8	0.736	3.74	33.1	0.696	2.93	22.0	0.866	3.56
33.2	0.686	3.64	21.3	0.665	2.88	16.1	0.850	3.68
21.4	0.654	3.64	15.5	0.646	2.88	10.2	0.832	3.93
15.5	0.634	3.64	9.59	0.624	2.99	7.21	0.820	4.21
9.64	0.614	3.84	6.67	0.610	3.14	4.28	0.796	5.06
6.71	0.602	3.94	3.75	0.595	3.73	3.12	0.783	5.45
3.78	0.587	4.68	2.58	0.590	4.42	1.98	0.760	6.30
2.61	0.582	5.04	1.42	0.582	5.40	0.87	0.720	7.87
1.47	0.567	6.40	0.29	0.566	6.50	-0.07	0.600	10.4
0.38	0.544	7.93	-0.44	0.440	8.50	-0.38	0.180	13.1
-0.45	0.445	9.20	-0.73	0.196	8.75	-0.48	0.000	13.1
-0.55	0.149	9.73	-0.83	0.000	8.75			
-0.66	0.000	9.73						

§ 5. Elastic Constants

At the same time, Young's moduli at magnetically saturated states, E_s , and at unmagnetized state, E_0 , were computed by using values for frequency, f_s and f_0 , corresponding to each state, and the length of the specimen as well as its density. They are given in Table 12.

According to the theory of elasticity, in cubic crystals such as nickel $1/E$, the reciprocal of Young's modulus, and κ , compressibility are expressed by the following relations:

$$1/E = S_{11} - 2\left(S_{11} - S_{12} - \frac{S_{44}}{2}\right)(\beta_2^2 \beta_3^2 + \beta_3^2 \beta_1^2 + \beta_1^2 \beta_2^2) \quad (7)$$

and

$$\kappa = 3(S_{11} + 2S_{12}), \quad (8)$$

where S_{11} , S_{12} and S_{44} are the elastic constants in Voigt's notation, and β_1 , β_2 and β_3 are direction cosines of the rod axis of the specimen with respect to the crystallographic tetragonal axes. Thus we tabulate values of $1/E_s$ and $1/E_0$ of various crystals in Table 12 and show $1/E_s$ as a function of $3I$ in

Table 12. Observed values of Young's modulus in nickel crystals.

E_s and E_o denote Young's modulus at the magnetically saturated state and at the unmagnetized state, respectively. $\Gamma (= \beta_2^2 \beta_3^2 + \beta_3^2 \beta_1^2 + \beta_1^2 \beta_2^2)$ is the orientation function.

Specimen number		Direction*	3Γ	E_s (dyne/cm ²)	E_o (dyne/cm ²)	$1/E_s$ (cm ² /dyne)	$1/E_o$ (cm ² /dyne)
				$\times 10^{12}$	$\times 10^{12}$	$\times 10^{-12}$	$\times 10^{-12}$
No.	1	[111]	0.9870	2.91	2.73	0.344	0.366
No.	2	[110]	0.7029	2.42	2.22	0.412	0.450
No.	3	[100]	0.0010	1.34	1.20	0.747	0.833
N	12a	[411]	0.3936	1.75	1.62	0.573	0.616
N	13a	[210]	0.5150	2.18	2.04	0.458	0.490
N	14a	[511]	0.2287	1.50	1.37	0.665	0.730
N	15	[100]	0.0244	1.40	1.26	0.716	0.794
N	17b	[100]	0.0334	1.36	1.24	0.734	0.805
Poly.				2.34	2.02	0.427	0.495

* See Fig. 2.

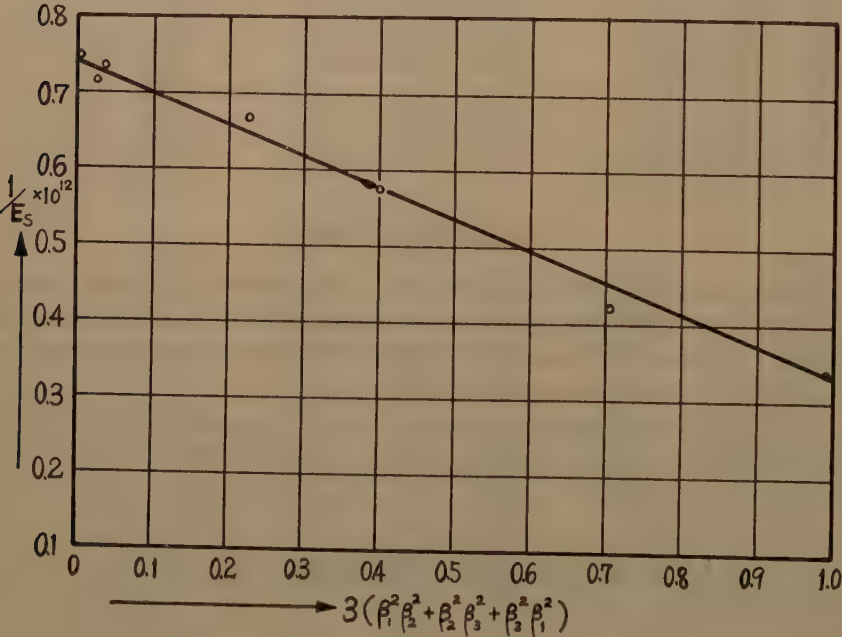


Fig. 10. The reciprocal of Young' modulus, $1/E_s$, at the saturated state as a function of the orientation function, 3Γ , in nickel crystals.

Fig. 10, where $\Gamma (= \beta_2^2 \beta_3^2 + \beta_3^2 \beta_1^2 + \beta_1^2 \beta_2^2)$ is the orientation function. Here 3Γ , three times of the orientation function, is taken by usage. As expected from (7) it is noted that these measured points are placed on a straight line

approximately. Substituting the values of $1/E_s$ into (7), we obtain values of S_{11} and $S_{11} - S_{12} - \frac{S_{44}}{2}$.

Further estimation for S_{12} and S_{44} , we intend to use the measured values of compressibility for polycrystalline nickel^[21]. In any metal, without distinction of the crystal lattice, the compressibility should be the same for a single crystal as for a polycrystal, since the compressibility of a single crystal does not depend upon the orientation. It may be reasonable if the effect of grain boundaries in the polycrystal is negligible and for some metals it has been testified. The most reliable experimental isothermal compressibility of polycrystalline nickel as determined by Bridgman^[22] and modified by Slater^[23] is the following value:

$$\kappa = 0.535 \times 10^{-12} \text{ cm}^2/\text{dyne}.$$

Substituting this value into (8), we can obtain S_{12} and further S_{44} . The results obtained are

$$\begin{aligned} S_{11} &= 0.73_8 \times 10^{-12} \text{ cm}^2/\text{dyne}, \\ S_{12} &= -0.28_0 \times 10^{-12} \text{ cm}^2/\text{dyne}, \quad (\text{Saturated state}) \\ S_{44} &= 0.81_4 \times 10^{-12} \text{ cm}^2/\text{dyne}, \quad (9) \end{aligned}$$

for nickel at the saturated state. The moduli of elasticity, C_{ij} , calculated by S_{ij} for nickel at the saturated state are given, too:

$$\begin{aligned} C_{11} &= 2.53_0 \times 10^{12} \text{ dyne/cm}^2, \\ C_{12} &= 1.54_8 \times 10^{12} \text{ dyne/cm}^2, \quad (\text{Saturated state}) \\ C_{44} &= 1.23_8 \times 10^{12} \text{ dyne/cm}^2. \quad (10) \end{aligned}$$

Further, the elastic anisotropy factor A is obtained by

$$A = 2 C_{44} / (C_{11} - C_{12}) = 2.50 \quad (\text{Saturated state}) \quad (11)$$

At the unmagnetized state, too, these values are computed by the same procedure as above. These are given as follows:

$$\begin{aligned} S_{11} &= 0.82_8 \times 10^{-12} \text{ cm}^2/\text{dyne}, \\ S_{12} &= -0.32_1 \times 10^{-12} \text{ cm}^2/\text{dyne}, \\ S_{44} &= 0.87_2 \times 10^{-12} \text{ cm}^2/\text{dyne}, \quad (\text{Unmagnetized state}) \\ C_{11} &= 2.46 \times 10^{12} \text{ dyne/cm}^2, \quad (12) \\ C_{12} &= 1.58 \times 10^{12} \text{ dyne/cm}^2, \\ C_{44} &= 1.14_5 \times 10^{12} \text{ dyne/cm}^2, \end{aligned}$$

and

$$A = 2.62$$

It should be stressed the fluctuations of the measured values of $1/E_0$ from the straight line in the $1/E_0$ vs I' curve are larger than that of $1/E_s$, and considered in § 6. The values obtained, (10), (11) and (12) are summarized in Table 13.

§ 6. Discussion

(A) Young's modulus and the elastic constants.

The elastic constants of nickel have been measured by several investigators. The data reported are summarized in Table 13. Among them, the data of Yamamoto²¹⁾, Honda and Shirakawa²⁴⁾, Shirakawa and Numakura²⁵⁾ are for

Table 13. Elastic constants (in 10^{12} dyne/cm²) of nickel crystals.

Investigators	Magnetically saturated			Unmagnetized			Remarks
	C_{11}	C_{12}	C_{44}	C_{11}	C_{12}	C_{44}	
This paper	2.53	1.55	1.24	2.46	1.58	1.14	*10 kc magneto-strictive vibration.
Bozorth et al. ⁶⁾	2.53	1.58	1.23	2.50	1.60	1.185	10 Mc ultrasonic pulsing method. (velocity measurement)
" 6)	2.524	1.538	1.23	2.52	1.54	1.229	"
" 6)	2.523	1.566	1.23	2.517	1.574	1.226	"
Neighbours ²⁶⁾	2.526	1.52	1.238				10 Mc ultrasonic pulsing method.
Yamamoto ²¹⁾				2.44	1.58	1.02	*20. kc magneto-strictive vibration.
Honda and Shirakawa ²⁴⁾				2.52	1.51	1.04	*Static loading method.
Shirakawa and Numakura ²⁵⁾				2.25	1.49	0.91	*Static loading method (calculated from S_{ij})

* Observed value of compressibility $\kappa=0.535 \times 10^{-12}$ cm²/dyne was used.

unmagnetized only and the variety of values may be expected, as shown in the table, because E_0 is sensitive to heat treatment and domain configuration. E_0 is, moreover, a function of the stress used. The larger to some extent the stress, the smaller E_0 is in general. The result of the static method shown in the table may be due to the larger stress used there. This should be also recognized in the results of the dynamic method. Therefore, it is necessary that a stress used should be as small as possible. It has already stated in § 3 that our measurements were carried out by the very small stress.

As already mentioned in § 1, therefore, in ferromagnetics the value at the saturation, E_s , is the normal Young's modulus. So the values of Bozorth *et al.*⁶⁾ and Neighbours *et al.*²⁶⁾ should be compared directly with the present result and agree well with each other, in spite of a difference in the method of measurements. (Frequency used is about 10 kc by us and 10 Mc by Bozorth and others.) For reference, reliable values for unmagnetized in our investigation are given, too; it is interesting that the change of C_{44} is the most remarkable. Accuracy of the absolute of E itself is worse than its relative change value $\Delta E/E$, of course, due to the difference of the measuring method; but the variety of the values for unmagnetized state is remarkable over the

experimental error, particularly in the direction of $[110]$.

(B) The change of Young's modulus with magnetization.

The forms of $\Delta E/E_s$ vs H curve and of $\Delta E/E_s$ vs I curve are different according to their orientation. Some peculiarities, found out about them, are quite similar to those on iron crystals qualitatively, as already reported by Yamamoto⁵⁾, replacing $[100]$ in iron to $[111]$ in nickel. Namely, in nickel as well as iron the behavior of the specimen with a direction of easy magnetization is almost like qualitatively, while with a direction of difficult magnetization it holds the same, too. But a consideration on this behavior, especially on unlike one, has not been carried on in detail.

The essential feature of the phenomena could be explained by the magnetic domain theory by considering two processes of the magnetostriction; rotations of the domain magnetization vector and displacements of the magnetic domain boundaries due to the applied stress. Becker and Döring²⁾, Döring¹³⁾ and Takagi¹²⁾ and others have proposed the domain theory on the ΔE effect.

As shown in Figs. 8 and 9, there are two stages of abrupt increase of the ΔE , near the residual point and just before the saturation. The latter, we consider, corresponds to the rotation process and, on the other hand, the former may correspond to the moving boundary process, as well. In this case the residual point may be a mark point which partitions both processes. Due to a mechanical vibration, however, the residual point may be affected and can not be decided as a point clearly in the experiment. Thus it is nothing but a marker, we suppose, near which the change due to the moving boundary process abruptly enlarges on the descending hysteresis curve. As a matter of fact, they are always found out near the middle point of the first increase of ΔE in the ΔE vs I curves, in Figs 8 and 9.

Table 14. Values of relative change of Young's modulus in nickel crystals. $(\Delta E/E_s)_r$ and $(\Delta E/E_s)_o$ are the values at the residual point and unmagnetized state, respectively. I is the orientation function.

Specimen number	Direction*	$3 I$	$(\Delta E/E_s)_o$ (%)	$(\Delta E/E_s)_r$ (%)
No. 1	$[111]$	0.9870	6.1	2.0
No. 2	$[110]$	0.7029	8.2	6.1
No. 3	$[100]$	0.0010	10.1	5.8
N 12a	$[411]$	0.3996	7.4	3.5
N 13a	$[210]$	0.5150	6.6	3.9
N 14a	$[511]$	0.2287	8.6	4.5
N 15	$[100]$	0.0244	9.8	6.2
N 17b	$[100]$	0.0334	8.9	5.8
Poly.			13.2	5.2

* See Fig. 2.

$(\Delta E/E_s)_r$, the values of $\Delta E/E_s$ at the residual point, and $(\Delta E/E_s)_0$ are tabulated in Table 14 and shown in Fig. 11 as a function of the orientation function. The values are found to be a straight line, that is, a linear function of $3I'$, as expected by the Döring's theory^{2,13}, but it is interesting that a remarkable deviation from the line has been found on the specimen with the direction of $[110]$ and $[210]$. A consideration on this anomaly is now in progress and will be reported in future.

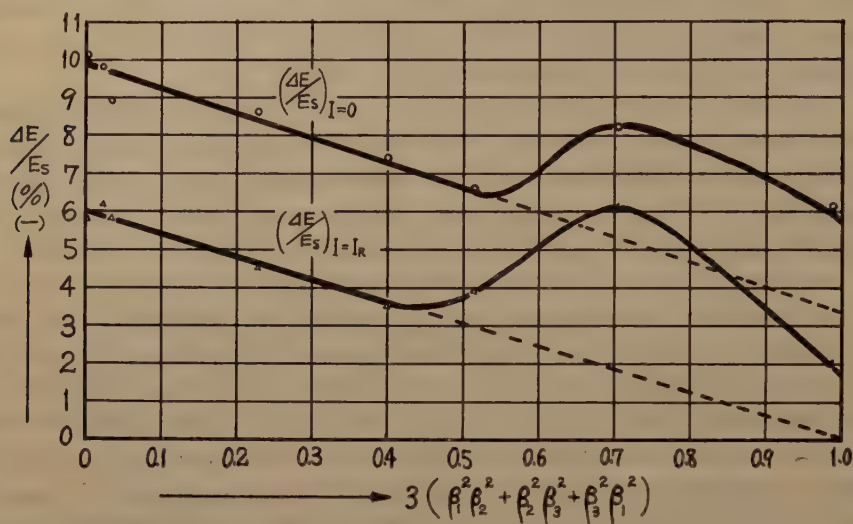


Fig. 11. $(\Delta E/E_s)_r$ and $(\Delta E/E_s)_0$ as a function of the orientation function.

(C) Frequency dependency.

According to Bozorth⁶, in his experiments at 10 Mc, the greatest change of Young's modulus was only about 3 per cent, while in usual resonance experiment at 10 to 20 kc, adopted also in our experiment, the value has been observed by 16 to 20 percent at room temperature. He has suggested this considerable distinction occurs due to relaxation of the domain wall motion by micro-eddy-current damping at higher frequency. The decrease of $\Delta E/E_0$ and the equivalent increase of the logarithmic decrement due to eddy-current damping with frequency for a polycrystalline nickel are shown in Fig. 12 after Bozorth⁶. The frequency used in our experiments is about 10 kc, where frequency dependencies of damping and $\Delta E/E_0$ are very remarkable as shown in the figure. Therefore, the cause of the variation of experimental $\Delta E/E$ value should be due to the variety of dimensions of the specimen, namely, the proper resonance frequency, and to the variety of domain size. In our experiment the unexpected result for a polycrystal, ΔE of which is larger than that for single crystals, could be explained by the eddy-current shielding theory to some extent. The thinner the sample and the smaller the domain size, the larger the ΔE effect should be observed. Whether the first abrupt

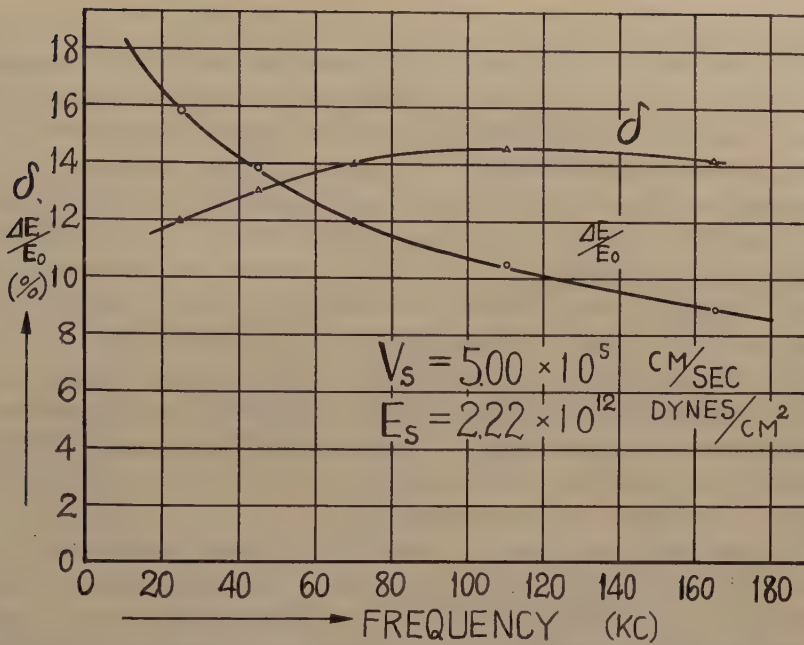


Fig. 12. Relative change in Young's modulus and the decrement, as a function of frequency for a polycrystalline nickel. (After Bozorth.)

increase near the residual point appears or not, therefore, is influenced by the eddy-current shielding due to higher resonance frequency, if the crystals were free from imperfection and strain.

§ 7. Summary

The nickel crystals of a slender cylindrical rod form were grown by the modified Bridgman's method in a molybdenum wound resistance furnace in a vacuum. (§2) Young's modulus and its change with magnetization, the ΔE effect, of the nickel crystals were measured by the dynamical method of magnetostrictive vibration at room temperature. The method of measurement and the construction of the measuring apparatus is described in detail. (§3) The results obtained are the followings:

(1) The normal value of Young's modulus in ferromagnetics is E_s , the value at the saturated magnetized state, where the magnetic domains are aligned all together and the additional magnetostrictive strain is negligibly small. Actually, E_s was determined uniquely in accordance with other investigators, while E_0 , the E -value at the unmagnetized state, was not as expected. Thus we took always E_s for a basic value and the customary measure of the magnitude of the ΔE effect was expressed as $\Delta E/E_s$, where $\Delta E = E - E_s$. A conversion formula from the expression $\Delta E/E_s$ to the ordinary expression

$\Delta'E/E_0$ was given. (§ 1, § 5, § 6)

(2) Generally, Young's modulus increased gradually with the increase of magnetization, but after the magnetization exceeded the residual point, the rate of increase once diminished remarkably, even showing a decrease in $[100]$, and then increased again very abruptly to the saturation. In $[111]$ the change was simple and the first step disappeared. This behavior was quite similar to that of iron crystals qualitatively, as already reported by Yamamoto⁵⁾, replacing $[100]$ in iron to $[111]$ in nickel. It was suggested that the first increase to the residual point was due to the moving boundary process, while the latter increase to the saturation was due to the rotation process. $(E/E_s)_r$, the value of $\Delta E/E_s$ at the residual point, was plotted as a function of the orientation function $3I=3(\beta_2^2\beta_3^2+\beta_3^2\beta_1^2+\beta_1^2\beta_2^2)$, where β_1 , β_2 and β_3 were direction cosines of the rod axis of a specimen referring to the crystal axes. The curve was found to be a straight line, excepting the specimens, $[110]$ and $[210]$. (§ 4, § 6)

(3) The elastic constants of nickel crystals were determined by using the data of $1/E$ in the single crystal and reliable experimental data of compressibility in polycrystalline nickel. The results obtained were $S_{11}=0.738$, $S_{12}=-0.280$ and $S_{44}=0.814\times 10^{-12}$ cm²/dyne at the saturated state. The moduli of elasticity were calculated to be $C_{11}=2.53_0$, $C_{12}=1.54_8$ and $C_{44}=1.23_8\times 10^{12}$ dyne/cm² at the saturated state. These values were directly compared with those obtained by means of velocity measurement of a 10 Mc pulse, and they coincided well with each other, in spite of a difference in the experimental method—in our case, resonance frequency measurement in about 10 kc region was used. (§ 5, § 6)

(4) Frequency dependence of Young's modulus was discussed briefly. (§ 6)

In conclusion, the authors wish to express their thanks to Prof. H. Takaki and the members of his laboratory of University of Kyoto who kindly gave advice and various conveniences in the preparation of nickel crystals, to Prof. M. Yamamoto of Tōhoku University and to Mr. N. Miyata of our laboratory for the helpful discussion and advice. The present work was partly supported by the Scientific Research Expenditure from the Ministry of Education.

References

- 1) K. Honda, S. Shimizu and S. Kusakabe: Phys. Z., **31** (1902), 380; Phil. Mag., **[6]** **4** (1902), 338.
- 2) R. Becker and W. Döring: *Ferromagnetismus*, Springer, Berlin (1939), p. 336.
- 3) R. M. Bozorth: *Ferromagnetism*, Van Nostrand, New York (1951), p. 684.
- 4) R. Kimura: Proc. Math.-Phys. Soc. Japan, **21** (1939), 686, 786; **22** (1940), 45, 219, 233.
- 5) M. Yamamoto: Sci. Rep. Tōhoku Imp. Univ., **31** (1943), 101.
- 6) R. M. Bozorth, W. P. Mason and H. J. McSkimin: Bell System Tech. J., **30** (1951), 970.

- 7) E. W. Lee: Rep. Prog. Phys., **18** (1955), 220.
- 8) Y. Nakamura: J. Phys. Soc. Japan, **10** (1955), 937.
- 9) N. Akulov and E. Kondorsky: Z. Phys., **78** (1932), 801; **85** (1933), 661.
- 10) M. Kersten: Z. Phys., **85** (1933), 708.
- 11) W. F. Brown: Phys. Rev., **50** (1936), 1165; **52** (1937), 325.
- 12) M. Takagi: Sci. Rep. Tōhoku Imp. Univ., **28** (1939), 85.
- 13) W. Döring: Z. Phys., **114** (1939), 579.
- 14) P. Bridgman: Proc. Am Acad. Arts Sci., **60** (1925), 305.
- 15) R. Glocker and L. Graf: Z. Anorg. Chem., **188** (1930), 232; L. Graf: Z. Phys., **67** (1931), 388.
- 16) H. Takaki, S. Nakamura, Y. Nakamura, J. Hayashi, H. Furukawa and M. Aso: J. Phys. Soc. Japan, **9** (1954), 204.
- 17) R. M. Bozorth, H. J. Williams and J. C. Walker: Rev. Sci. Inst., **20** (1949), 947.
- 18) R. F. Pearson: Brit. J. Appl. Phys., **4** (1953), 115.
- 19) M. Yamamoto: Sci. Rep. Tōhoku Imp. Univ., **27** (1938), 342.
- 20) O. Engler: Ann. d. Physik, **31** (1938), 145.
- 21) M. Yamamoto: Sci. Rep. Res. Inst. Tōhoku Univ., **3** (1951), 308; Phys. Rev., **77** (1950), 566.
- 22) P. W. Bridgman: Proc. Am. Acad. Sci., **58** (1923), 165.
- 23) J. C. Slater: Phys. Rev., **57** (1940), 744.
- 24) K. Honda and Y. Shirakawa: Sci. Rep. Res. Inst. Tōhoku Univ., **1** (1949), 9.
- 25) Y. Shirakawa and K. Numakura: Nippon Kinzoku Gakkai-Shi, **19** (1955), 99 (in Japanese).
- 26) J. R. Neighbours, F. W. Bratten and C. S. Smith: J. Appl. Phys., **23** (1952), 389.

日本附近における上層低気圧と 地表低気圧との関係

On the Relations between High-Level Cyclones and
Surface Cyclones near Japan

増 井 次 夫 T. MASUI

Abstract

A high-level cyclone is formed from a pre-existing upper trough by cutting-off process, as examined by E. Palmén. The principal source region of the high-level cyclones which have any effect on the weather of Japan is Southeast Siberia or Northeast China except in the Baiu Season. Occasionally in the Baiu Season (June-July) the source region moves westward. In most cases, one or two surface cyclones develop in front of the same trough at lower latitudes, namely on the Yellow Sea or the East China Sea. At first the high-level and surface cyclones situate apart. In general, high-level cyclones move towards the southeast, and surface cyclones towards the northeast. When they go on to the east of Japan, they gradually approach towards each other and mostly merge into a deep cyclone which makes its way to the North Pacific Ocean or the Sea of Okhotsk as an intense cyclone. The process to merging here is very complex; in this paper, therefore, the author has mainly investigated the tracks of cyclones, based on the data from 1951 to 1955, without dealing with the process in detail.

緒 言

日本附近における低気圧については既に多くの人々により論ぜられ、その発生及び発達過程に関し大部分の場合は J. Bjerknes の前線論で説明されるものと考えられていた。しかし高層気象及び高層風観測法の進歩、観測網の整備と共に、偏西風 trough の中に発生する上層低気圧 (high-level cyclone 或は cold vortex または cut-off low) が強い影響を持つことが次第に明らかにされて来た。(勿論地表低気圧の発達を促すものは上層の深い trough であるが、trough が深い場合には概ね上層低気圧を伴うので本文では上層低気圧を以て代表させた。従つて上層低気圧の現れてない trough に関連して地表低気圧が発達する場合もある。)

一般に顕著な地表低気圧 (下層低気圧) は偏西風 trough (このtrough は問題の上層低気圧の trough より一つ先のもののこともある) の前面の発散域に発生することがよく知られている。しかしその発生域については地形の影響をうけることが大きく、

日本附近では偏西風 trough が西方より大陸東岸に接近したときその海上に発生することが多い。即ち低気圧の主要発生地は台湾附近（代表的のものは「台湾坊主」と呼ばれる）、東支那海または黄海附近であるが、季節によつては（主に梅雨期）それ以西の中国低地地方に発生することもある。

これらの低気圧の他に大陸内部（主として Baikal 湖附近）に現われ南東または東南東に進み黄海北部または日本海に進行して来るものも相当に多いが（通常「大陸旋風」と呼ばれる）、この低気圧は後に示すように直接上層低気圧に関連することが多い。

一般に日本西方の偏西風 trough の前面に発生した地表低気圧は最初は東進し、次第にその方向を変え、東北東から北東に向つて進行するものが大部分である。しかし地表低気圧から発達し単独に上層（500 mb）までのびるものは比較的少ない。多くの低気圧は日本中部以東の経度で急速に発達するが、この場合大きい影響を持つものは大陸から南下してきた深い上層低気圧で、相互の径路の接近と共に両者は次第に合流し、背の高い低気圧として北東進することが多い。この点については J. Bjerknes も既に述べている。その際の地表低気圧の示度の低下は急激で、時として 50 mb 以上に達することがある。（第 3 図）

台風の進路も偏西風 trough と深い関係があるが、ここに述べる上層低気圧とは直接関係することが少ないので、ここでは問題にしないこととする。

本文では主として両者の径路の関係につき 1951 年春期から 1955 年終りまでの、少々顕著な地表低気圧または上層低気圧の存在した場合を調査したので、見落した場合も幾分はあると思う。主な資料は中央気象台発行の極東天気図、気象要覧、Aerological Data 並びに高層天気図及び 1952 年末までの Weather Bureau 発行の Synoptic Weather Maps からとつた。

日本附近における上層低気圧

成 因： 最近約十年間中国における資料が入手し得ないので Asia 大陸東部における上層低気圧（寒冷低気圧）の成因については明瞭でないところが多いが、北半球高層天気図等から推察すると、その成因は、E. Palmén 及びその他の人々により論ぜられた北半球の他の地域即ち北米大陸、欧州方面及びその他の地方に発生するものと大差なく、偏西風波動の振巾の増大により主流から cut-off をされた寒気によるものと考えられ、東亞におけるものも構造上の特異性は少ないようである。しかし東亞においては発生する地域はかなり限定されているように思われる。

日本に影響を与える上層低気圧の発生地域は一般に 120° E またはそれ以東で、梅雨期及びその前後においてのみ稍々西に偏ることがある。即ち大部分は Baikal 湖附近から中国北東部（蒙古、北支那、満洲）の地域で、時として沿海州附近がその発生地となる。

第 1 図に示すものは日本海に南下したもので、その径路は第 10 図に示してある。

上層低気圧の発生地が東亞においてかなり限定されていることについて考えられることは Himalaya 山脈を含む Asia 大陸の高地による偏西風波動の特異性である。これ

らの高地は地球をとりまく大きい jet stream の位置をかなり限定し、その東端附近に大きい trough をつくることが多いと思われる。寒候期においては subtropical jet stream の主流は Himalaya 山脈の南側を吹走し、日本後近で最も南に偏すると共に最強流となる。その際 polar front jet stream も Siberia 中部から中国北東部を径て南下し日本附近に大きい trough をつくることが多い。勿論これは平均的な傾向ではあるが低気圧の発生地域を大いに支配する。大陸内部における偏西風 trough の東進が天気図上で認められる場合も多いが顕著な上層低気圧が中国中部を通過した例はあまりないようである。

梅雨期においては偏西風の風力も全体として弱まり偏西風 trough の位置が少々西偏することも可能と思われる。しかしこれらの関係については資料不足のため確定的なことは述べられない。

発生回数： 季節的な特長は明瞭には認められないが春秋に少々多く、特に日本の北東方に blocking high が存在するときは上層低気圧が続発する傾向がある、従つて梅雨期にも多い。

径路： 日本附近に南下する上層低気圧の径路は梅雨期及びその前後を除きあまり季節的な特長はない。径路はかなり頻繁に変化するが、一径路を二つの上層低気圧が引続き通過することも多い。最も南まで下るものは中国北東部から日本中部を横切り太平洋まで出るもので、その際の寒気の頂は著しく降下し下層に前線を形成することもある。しかしこのような場合は比較的に少ない。日本の北東方に顕著な blocking high が出現するときはその南側の周辺を回る傾向が見られ、特に梅雨期には著しい。しかし梅雨期においても日本より西方の径路は不明瞭の場合が多く、黄海附近または中国の平地地方に南下しその後黄海、日本海を東北東に進むものが多いように思われる。勿論梅雨期でも他の径路をとるものも多い。

一般に径路は拋物線状で、緯度 $35^{\circ}\sim 50^{\circ}$ N. 経度 $130^{\circ}\sim 145^{\circ}$ E の地域に頂点を持つものが多い。複雑なものは途中で loop を画くこともあり、また一度南下して更に太平洋に入ってから再び南東に進むものもある。後者の場合日本列島に沿い暖気の移流が顕著なことが多い。loop を画く場合地表低気圧との関連は複雑であるが、地表低気圧自身の発達には著しくはない。(上層低気圧も発達しないことが多い)。日本の北東方に blocking high が出現したとき上層低気圧が東進せず、その西側で北進し消滅する場合もある。この際北側の地表低気圧もこれに附随した径路を画く。

地表低気圧が発達し易い順に上層低気圧の径路を分類すると大体次のようになる。

- (1) (満洲北部)―沿海州―北日本―北太平洋(または Okhotsk 海)。この場合地表低気圧は日本をはさんで「二つ玉」として発達することが多い。
- (2) 中国北東部(満洲)―日本海―北太平洋。この場合も地表低気圧が発達し易い。
- (3) (中国北部)―貴海―日本海―北日本―Okhotsk 海(または北太平洋)。梅雨期に多く現われ地表低気圧は少々発達したまま東北東に移動する。それ以上発達することは少い。
- (4) 中国北東部―日本海西部―日本中部―北太平洋。数は少いが太平洋岸で地表低

気圧が発達することがある。

(5) 日本以東に南下してくる場合。数は少い。この場合は日本の天気への影響は殆んどない。

(6) 種々複雑な経路を画く場合。

以上のうちでほぼ同一経路を引続き二つ以上の上層低気圧が進行しているときは対応する地表低気圧の発生及び経路は複雑となる。

進行速度： 進行速度に関しては明瞭な特長はないが頂点附近でやや低速になる傾向を示すものもある。loop を画く場合は特別で停滞状態に近い。一般には偏西風の速度に支配されるものと思われる。

上層低気圧の予報： この問題は数値予報の立場からいくつかの例について取扱われ、よい結果が得られている。しかし地表低気圧との関連については本文で見られるようにかなり複雑であるから注意を要する。

日本附近の上層低気圧の性情・構造については本文においては述べず、別の機会に扱うこととする。本文においては主としてその経路について地表低気圧との関係を取扱う。

日本附近における地表低気圧

地表天気図から見ると日本附近の地表低気圧は大体次の三種類に分けられる。

(1) 大陸東部の偏西風 trough の前面で発生し、最初は東進し、次第に北東に向きをかえて行くもの。この場合は急速に発達するものが多い。従つて日本本土及び海上では被害が多い。

(2) 大陸内部から南下東進し日本海附近に現われ次第に向きをかえて北東に進むもの。(大陸旋風)

(3) 台風または熱帯低気圧。

このうち (3) は上層低気圧とは直接の関係が少いので除外する。最も問題となるのは (1) である。(2) は日本本土南西部ではあまり関係なく北日本で被害を生ずることがある。

(1) に属するものは主として台湾附近の海上一多くは東支那海(「台湾坊主」)に発生するが南支那海で発生することもあり、北では黄海にも発生する。発生する場合は、西方上空に偏西風 trough があり地表附近には明瞭な不連続線がある場合が多い。発生後の発達には海面上の多量の水蒸気が影響する。(1) に属する低気圧のうちで発生地域が偏西風中の南北二カ所にあり、両者殆んど同時に発生し日本本土をはさんで東北東に進むものは「二つ玉」と呼ばれ降水量が多く日本の天気に大きい影響を与える。これらが北東に進んだ場合発達した上層低気圧と合流し急に発達することが多い。時として日本海側のもののみ上層低気圧と合流し、太平洋側のものは単独に上層迄発達することもあるが、この場合には日本北東方に急激に強い blocking high が出現していることが多い。

「二つ玉」としてではなく日本海に大陸旋風があり、太平洋側に地表低気圧が北東に

進行して合流する場合もある。またこの場合地表低気圧が日本海側のみのこともある。これらの地表低気圧の発達には上層低気圧の発達と関連することは勿論である。

地表低気圧の示度の低下は極端な場合は 50 mb 以上に達するが大部分は 20 mb 前後である。形の上では同様な径路をとつても、上層低気圧が衰弱するときは地表低気圧も発達しないこともあり、また地表低気圧だけでかなり発達する場合もある。

(2) の場合は一般に地表低気圧としてはあまり強力でない場合が多く閉塞型の低気圧として現れる。日本南部の天気には大きい影響を与えずむしろ日本南部は高気圧圏内に入ることが多い。(不連続線だけは通過する場合がある)。

この低気圧と上層低気圧との関係は密接でむしろ地表低気圧は上層低気圧に附随するものと考えてよい。この低気圧については既に E. Palmén が論じている。

上層低気圧が主導する場合には地表低気圧が陸地を「またぐ」という現象がよく見られる。即ち朝鮮半島または日本を横切の場合に地表低気圧はその西岸で次第に衰弱消滅すると共にその東側に新に発生し発達しながら東進する。

(1) と (2) とが単独でなく複合の形で発生することも勿論多い。また一つの上層低気圧が通過するとき幾通りかの地表低気圧が発生しそれぞれ東進する場合もあるが、このような場合地表低気圧の発達は著しくはないのが普通である。また上層低気圧が現れても地表低気圧が発生しにくい場合もある。

地表低気圧と上層低気圧とが密接に関連する場合の例

(1) 地表低気圧が「二つ玉」で、上層低気圧が満洲から日本海に南下東進した場合。1953 年 3 月 25 日～29 日に現れたもの。第 2 図に示すように日本海を東進した地表低気圧の方が先に発達したが後に太平洋側のものに合併し更に上層低気圧と合流、27 日 15 時には 982 mb まで示度が深まつた。その後は次第に衰弱している。

第 3 図に示すように 1955 年 2 月 20 日～22 日に現れたものでは上層低気圧は最初二つに分れていて日本海北部で合併し大きなものとなつている。進路は宗谷海峡から Okhotsk 海に向つている。地表低気圧は日本海側のものが発達し太平洋側のものを吸収し上層低気圧と合流してから示度は 950 mb (示度の低下 56 mb) まで下つている。全般の姿勢は次の (2) の場合に近い。これだけの発達は珍しい。

(2) 地表低気圧が東支那海から日本海を北東進し、沿海州から南東に進んできた上層低気圧と合流し急速に発達した場合。第 4 図に示すように 1954 年 5 月 9 日～11 日に現れたものでは地表低気圧の示度の降下は約 48 mb に達し北海道方面に大きい被害を生じた。この場合、上層低気圧の発達は数値予報の好例として発表されている。

(3) 大陸旋風の例。第 5 図に示したものは 1952 年 4 月 17 日～20 日に現れ、地表低気圧が先行し北日本海で示度が最低になつている。この場合は上下低気圧は同軸で、その傾きが問題となろう。

(4) 梅雨期の例。第 6 図。期間 1953 年 5 月 28 日～31 日。地表低気圧の示度降下はあまり急ではない。これは季節特有の性質である。第 7 図は、1954 年 6 月 5 日～8 日に現れたもので地表低気圧の径路は少々複雑である。6 日以前の上層低気圧の

動向は明らかでない。

(5) 上層低気圧が日本本上中部まで南下した場合。第8図 a 及び b は 1952 年 3 月 22 日～28 日に出現したもので、a は上層低気圧の径路、b は地表低気圧の径路を示す。上層低気圧 2 個が前後して進み、日本北東方海上に出てから前のものは北北西に回つて消滅、後のもののみ発達しながら北東に進んでいる。これに伴い地表低気圧の動きも複雑である。後の上層低気圧が日本本上を横断した際太平洋岸に急に地表低気圧が出現し北東に進行し次第に発達 (970 mb まで) している。最低圏界面高度 500 mb (3 月 24 日 12 時 米子)。

第9図は 1955 年 12 月 24 日～28 日に現れたものであるが上層低気圧は太平洋に出てから分裂北上し衰弱している。

(6) 上層低気圧が複雑な径路を画いた場合。第10図。期間 1952 年 3 月 9 日～12 日。上層低気圧が北朝鮮東部で一度 loop を画く。これに伴う地表低気圧の動向は複雑である。

第11図。期間 1952 年 6 月 3 日～8 日。これら両者共低気圧の強い発達はない。

第12図。期間 1954 年 11 月 27 日～12 月 3 日。上層低気圧が二段に南下し日本の東南東太平洋上で停滞した。しかし停滞期間中の上層低気圧の動向については資料不足のため図示し得ない。この場合、上層低気圧の後面において日本列島に沿う南西風の移流がかなり強い。

第12図。期間 1954 年 7 月 13 日～21 日。一度北東に進んだ上層低気圧が再び南東に進んで停滞した。この際南西から温暖高気圧が張出して来ている。

結 び

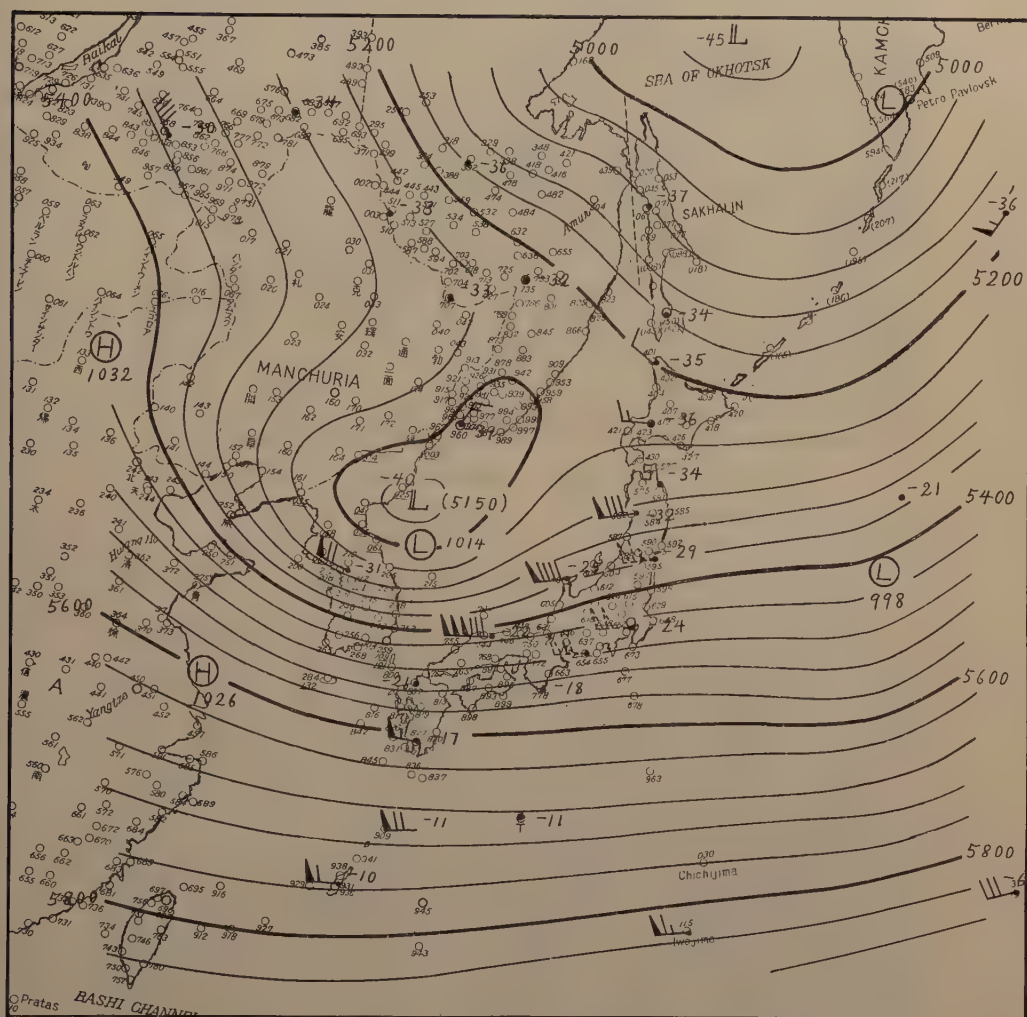
地表低気圧と上層低気圧との関係は前述の如く様々な場合があり簡単には把握し得ないが、上層低気圧に着目すると複雑な地表低気圧の動向が比較的容易に予想し得る場合がある。しかし偏西風の弱い時期においては取扱いにくい場合も多い。特に梅雨期においては大陸内部の資料の入手が望ましい。

終りに資料に関し多大の便宜を与えられた中央気象台の方々に厚く感謝の意を表する次第である。

文 献

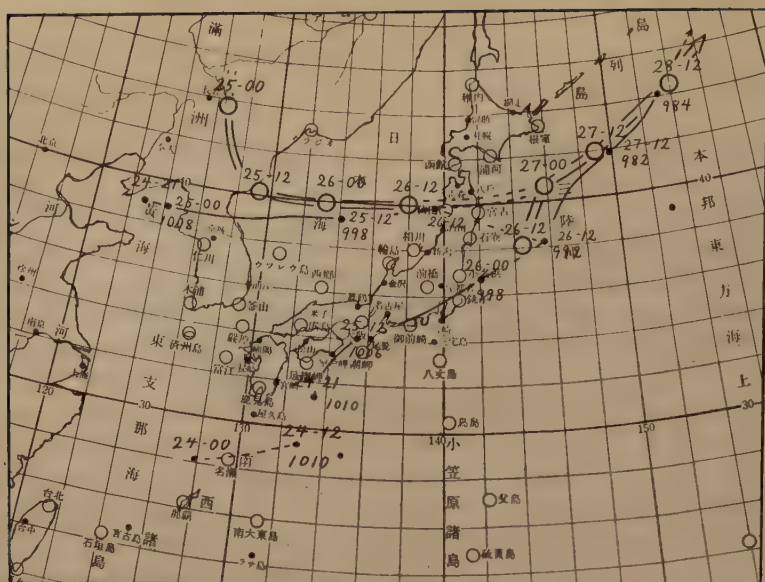
- Crocker, A. M., Godson, W. L., and Penner, C. M., 1947: Frontal Contour Charts. Journ. Met. 4, 95～99.
- Hsieh, Y. P. 1949: An Investigation of a Selected Cold Vortex over North America. Journ. Met. 6, 401～410.
- Palmén, E., 1949: On the Origin and Structure of High-Level Cyclones South of the Maximum Westerlies. Tellus, 1, 22～31.
- Palmén, E., 1951: The Aerology of Extratropical Disturbances. Compendium of Meteorology, 599～620.
- Bjerknes, J., 1951: Extratropical Cyclones, Compendium of Meteorology, 577～598.

- 村上多喜雄, 1951: 梅雨あけの機構, 気象集誌, 29, 162~175.
- Ooi, S., Matsumoto, S. and Itoo, H., 1951: A Study on the Westerly Troughs near Japan. Pap. in Met. and Geophys. 2, 219~233.
- Saito, N., 1953: An Aerological Study of the Cold Vortex and Stationary Front in Summer in the Far East. Journ. Met. Soc. of Japan, 31, 51~59.
- 沢田竜吉, 1947: 上層, 中層及び下層低気圧に就いて, 気象集誌, 25, 71~106.
- Scherhag, R., 1948: Neue Methoden der Wetteranalyse und Wetterprognose. Berlin Springer-Verlag, 1948. p. 227.
- Staff Members of the Dept. of Met. of Univ. of Chicago, 1947: On the General Circulation of the Atmosphere in Middle Latitudes, A Preliminary Summary Report. Bull. Amer. Met. Soc., 28, No. 6. 255~280.
- Suda K. and Asakura, T., 1955: A Study on the Unusual "Baiu" Season in 1954 by Means of Northern Hemisphere Upper Air Mean Charts, Journ. Met. Soc. of Japan, 33, 233~244.
- Suda K., 1955: On the North-High Situation in the Far East as a Link of World Pressure Distribution. Reports of the University of Electro-Communications, No. 7.
- Gambo, K., 1956: The Topographical Effect upon the Jet Stream in the Westerlies. Journ. Met. Soc. of Japan. 34, 24~28.
- 岸保勘三郎, 真鍋淑郎, 1955: 数値予報の基礎, 天気 2, 4~5 号.
-



第 1 図 500—mb 天気図, 1952年3月11日00時

- 印 地表低気圧及び高気圧
- LL 上層低気圧

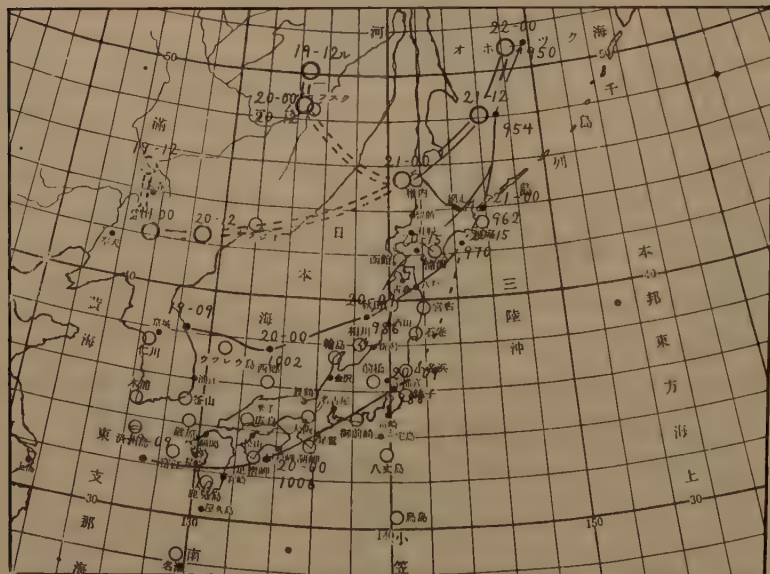


第 2 図 低気圧経路 1953 年 3 月 25 日~28 日

○ 上層低氣压 = 上層低氣压徑路

● 地表低氣压 — 地表低氣压徑路

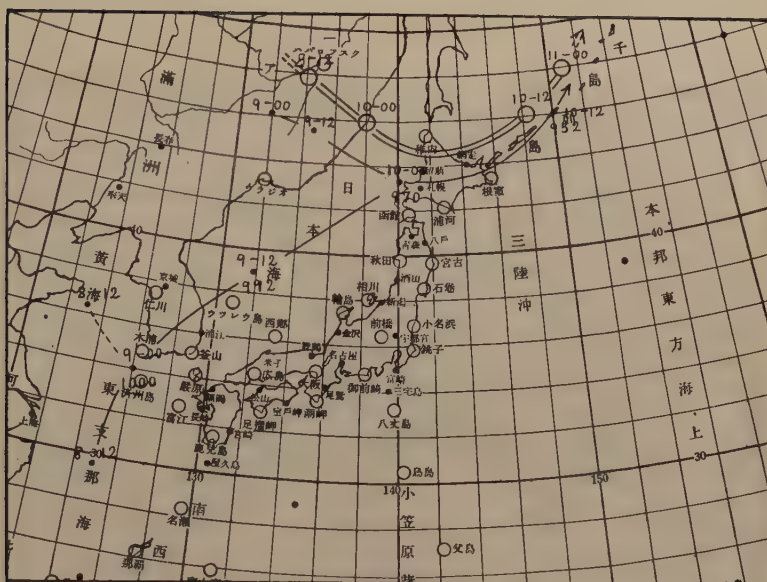
上層低気圧の位置は 500 mb 天気図における中心の位置である。以下同じ。



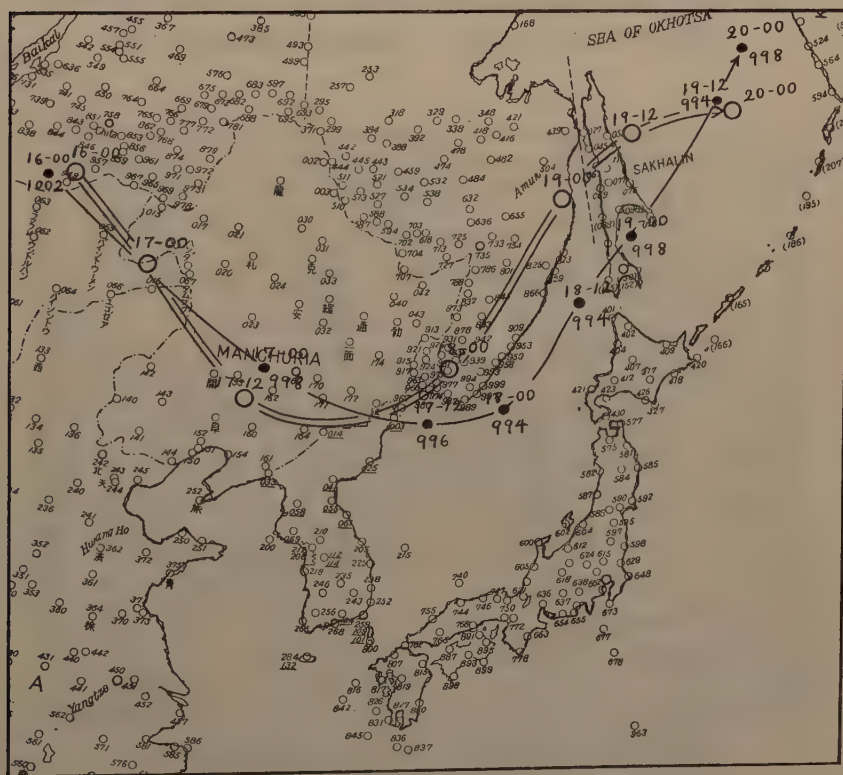
第 3 図 低気圧経路 1955 年 2 月 19 日~22 日

○ 上層低氣压 = 上層低氣压徑路

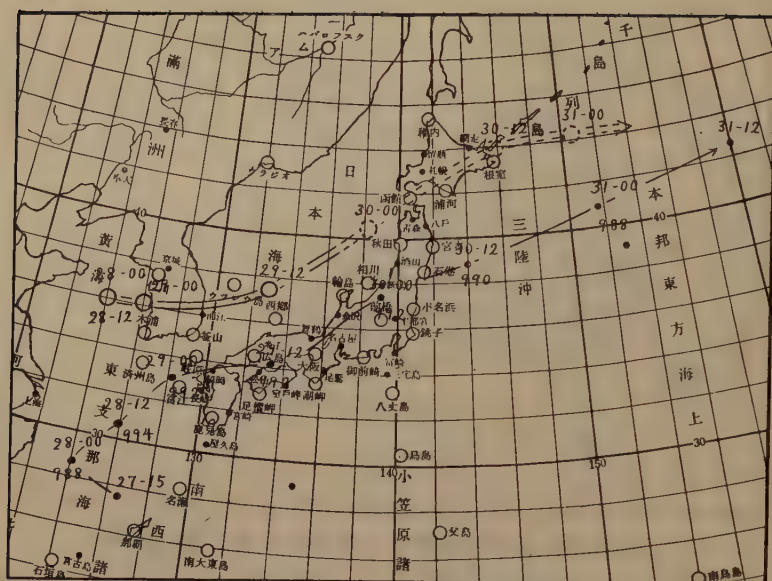
● 地表低氣压 — 第表低氣压徑路



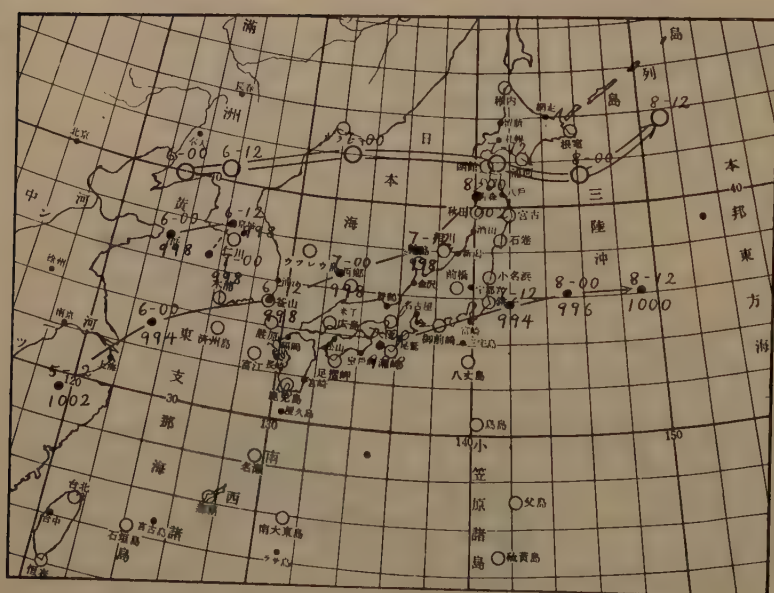
第 4 図 低気圧径路 1954 年 5 月 9 日~11 日



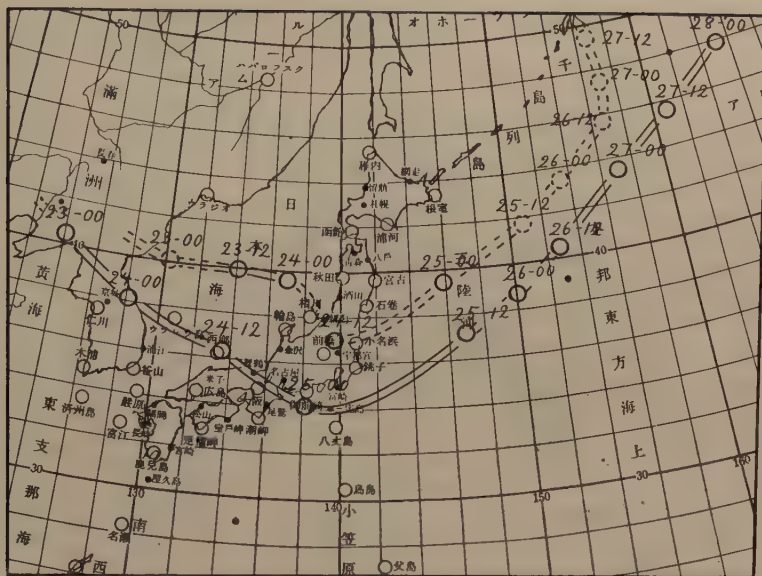
第 5 図 低気圧径路 1952 年 4 月 17 日~20 日



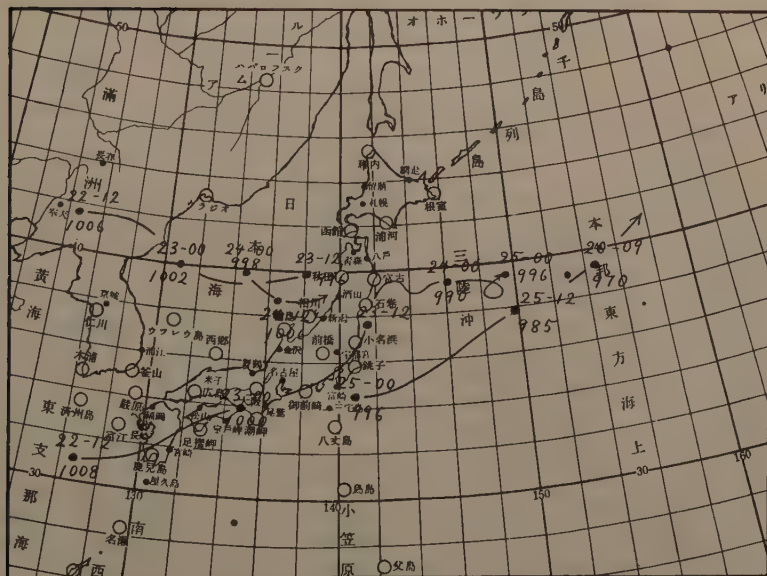
第 6 図 低気圧径路 1953 年 5 月 28 日~31 日



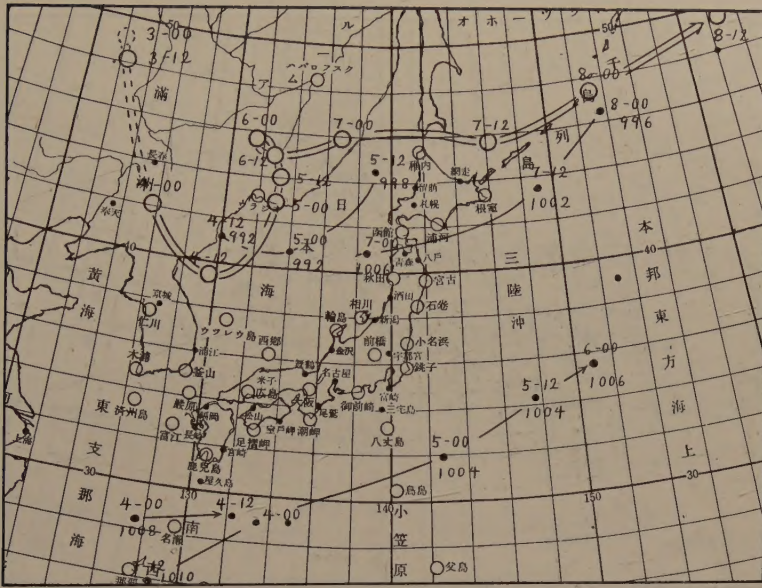
第 7 図 低気圧径路 1954 年 6 月 5 日~8 日



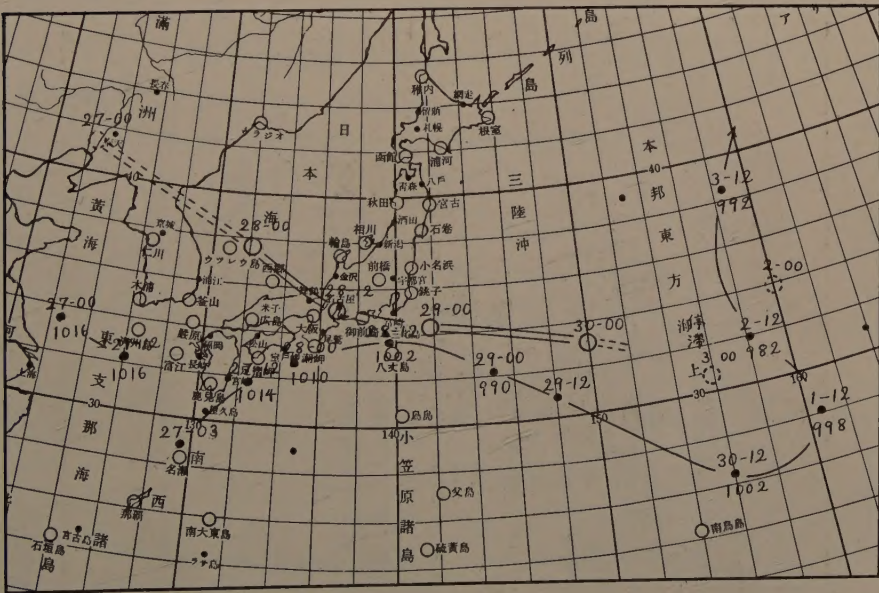
第 8 図 a. 上層低気圧径路 1952 年 3 月 23 日~28 日



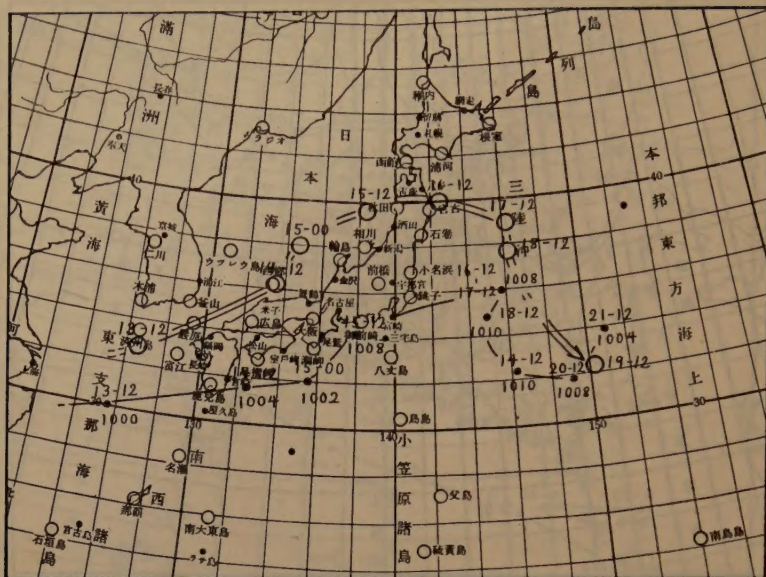
第 8 図 b. 地表低気圧径路 1952 年 3 月 23 日~28 日



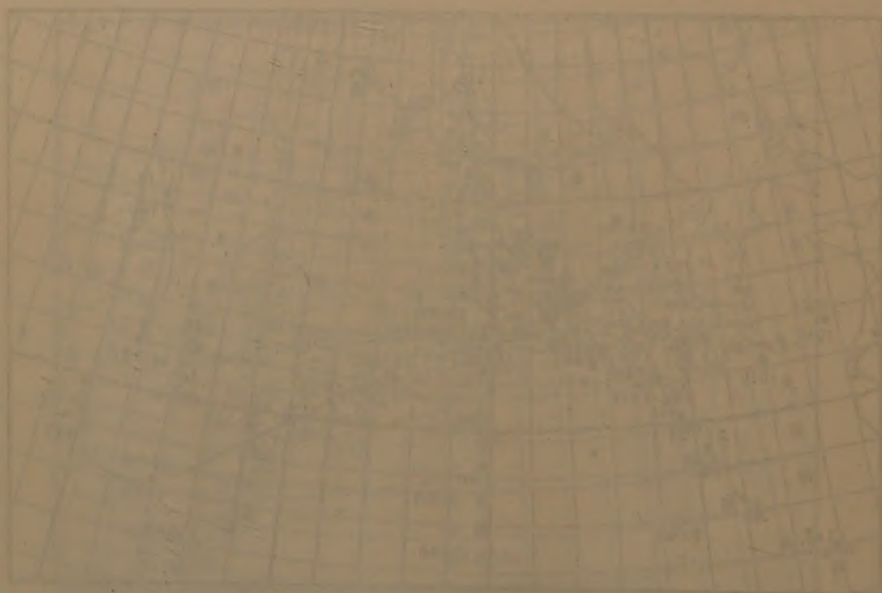
第 11 図 低気圧径路 1952 年 6 月 3 日～8 日



第 12 図 低気圧径路 1954 年 11 月 27 日～12 月 3 日



第 13 図 低気圧径路 1954 年 7 月 13 日~21 日



日本気象協会 気象情報 1954 年 7 月 13 日~21 日

昭和三十一年九月十八日印刷
昭和三十一年九月二十日発行

横浜市南区大岡町
編輯兼 横浜国立大学
発行者

東京都港区芝浦一ノ
印刷者 富 田 元

東京都港区芝浦一ノ
印刷所 ヘ ラ ル ド 社

CONTENTS

On n -dimensional projectively flat spaces admitting a group of affine motions of order $r=n^2-n+1$	Yosio MUTŌ.....	1
Effects of Humidity on Lichtenberg Figures.....	Bunji ARAI.....	16
Hexagonal Steps on the Surface of F_3O_4 solidified from the Melt	Nahonori MIYATA and Yasuo GONDŌ.....	27
Precision Density Measurement of Nickel-Copper Alloys. Part I	Yasuo GONDŌ, Nahonori MIYATA and Tetsuo KAMENO.....	29
Variation of Young's Modulus with Magnetization in Single Crystals of Nickel	Toshirō WATANABE, Yasuo GONDŌ and Zenya FUNATOGAWA.....	36
On the Relations between High-Level Cyclones and Surface Cyclones near Japan.....	T. MASUI.....	58